PPPL--2386

DE87 003065

PLASMA-MATERIAL INTERACTIONS IN TFTR

H.F. Dylla, M.G. Bell, W.R. Blanchard, F.P. Boody, N. Bretz, R. Budny, C.E. Bush,[a] J.L. Cecchi, S.A. Cohen, S.K. Combs,[a] S.L. Davis, B.L. Doyle,[b] P.C. Efthimion, A.C. England,[a] H.P. Eubank, R. Fonck, E. Fredrickson, L.R. Grisham, R.J. Goldston, B. Grek, R. Groebner,[c] R.J. Hawryluk, D. Heifetz, H. Hendel,[d] K.W. Hill, S. Hiroe,[a] R. Hulse, D. Johnson, L.C. Johnson, S. Kilpatrick, P.H. LaMarche, R. Little, D.M. Manos, D. Mansfield, D.M. Meade. S.S. Medley, S.L. Milora,[a] D.R. Mikkelsen, D. Mueller, M. Murakami,[a] E. Nieschmidt,[e] D.K. Owens, H. Park, A. Pontau,[b] B. Prichard, A.T. Ramsey, M.H. Redi, J. Schivell, G.L. Schmidt, S.D. Scott, S. Sesnic, M. Shimada,[g] J.E. Simpkins,[a] J. Sinnis, F. Stauffer,[f] B. Stratton, G.D. Tait, G. Taylor, M. Ulrickson, S. von Goeler, W.R. Wampler[b], K. Wilson,[b] M. Williams, K.L. Wong, K.M. Young, M.C. Zarnstorff, and S. Zweben

Plasma Physics Laboratory, Princeton University

P.O. Box 451, Princeton, NJ 08544

[a]Permanent address: Oak Ridge National Laboratory, Oak Ridge, TN
[b]Permanent address: Sandia National Laboratory, Livermore, CA
[c]Permanent address: GA Technologies, Inc., San Diego, CA
[d]Permanent address: RCA David Sarnoff Research Center, Princeton, NJ
[e]Permanent address: EG&G, Idaho
[f]Permanent address: University of Maryland, College Park, MD
[g]Permanent address: Japan Atomic Energy Research Institute, Japan

Key Words: TFTR, Impurities, Recycling

Abstract

This paper presents a summary of plasma-material interactions which influence the operation of TFTR with high current ($\lesssim$ 2 MA), ohmically heated and high power ($\sim$ 10 MW), neutral-beam-heated plasmas. The conditioning procedures which are applied routinely to the first-wall hardware are reviewed. Fueling characteristics during gas, pellet, and neutral beam fueling are described. Recycling coefficients near unity are observed for most gas-fueled discharges. Gas-fueled discharges after helium discharge conditioning of the toroidal bumper limiter and discharges fueled by neutral beams and pellets show $R < 1$. In the vicinity of the gas-fueled density limit (at $n_e = 5\text{-}6 \times 10^{+19} m^{-3}$) values of Z_{eff} are $\lesssim 1.5$. Increases in Z_{eff} of $\lesssim 1$ have been observed with neutral beam heating of 10 MW. The primary low-Z impurity is carbon with concentrations decreasing from $\sim$ 10% to $<$ 1% with increasing n_e. Oxygen densities tend to increase with n_e, and at the ohmic plasma density limit oxygen and carbon concentrations are comparable. Chromium getter experiments and He^{++}/D^{+} plasma comparisons indicate that the limiter is the primary source of carbon and that the vessel wall is a significant source of the oxygen impurity. Metallic impurities, consisting of the vacuum vessel metals (Ni, Fe, Cr), have significant ($\sim 10^{-4}\ n_e$) concentrations only at low plasma densities ($n_e < 10^{+19} m^{-3}$). The primary source of metallic impurities is most likely ion sputtering from metals deposited on the carbon limiter surface.

Invited paper presented at the Seventh International Conference

on Plasma-Surface Interactions in Controlled Fusion Devices

Princeton, NJ, May 5-9, 1986

1.0 INTRODUCTION

Plasma-material interactions significantly affect the present operation of TFTR. Understanding these interactions and their coupling to the edge plasma parameters is necessary to optimize future TFTR results. This paper documents the considerable effort expended on plasma-material issues, such as conditioning, impurity control, and fueling studies for the operation of TFTR with high current ($I_p \leq 2.2$ MA), ohmically heated and high power (~ 10 MW), neutral-beam-heated plasmas. These activities have paced the evolution of the machine as substantial new first-wall hardware has been added, and as the auxiliary heating power has been increased from 5-7 MW in early 1985 to the present level of 10-15 MW. The neutral beam power should peak at 20 MW late in 1986, followed by an upgrade in power to 27 MW in 1987.

The conditioning procedures which are applied routinely to the first-wall hardware in TFTR following venting of the torus to atmosphere are reviewed and updated (Section 2.0) from previous publications [1,2]. In addition to the use of standard glow discharge and pulse discharge cleaning techniques, we describe a disruptive discharge cleaning technique which was found necessary to condition the recently installed graphite bumper limiter. Active impurity control techniques incorporated during the course of high power plasma operation include gettering experiments with a prototype ZrAl surface [3] pumping array and with evaporative Cr gettering [4].

Measurements of the plasma impurity content and modelling of the impurity source mechanisms are presented in Section 3.0. The variation of both low-Z (primarily C and O) and high-Z impurities (Ni, Fe, Cr) with input power, plasma density, plasma current, and fuel gas (H, D or He) has been studied. Three-dimensional calculations of the sputtered flux have been performed to assess the importance of ion sputtering of the limiter as an impurity source mechanism.

The plasma fueling and recycling behavior with gas, pellet and neutral beam fueling are described in Section 4.0. Recycling coefficients and global particle confinement times are inferred from particle input, H_α, and Langmuir probe measurements. Recycling coefficients are generally near unity for gas-fueled discharges. For pellet and neutral-beam-fueled discharges, the recycling coefficient drops significantly below unity. For a special case of gas-fueled operation on the bumper limiter, density pumpout, which can be ascribed to decreased recycling, has been observed. The implications of this limiter pumping effect on the future requirements for edge profile modification in TFTR are described. Finally, in Section 5.0 a summary of the above results is given.

For reviews of the results of plasma confinement and heating studies in TFTR, the reader is referred to several recent conference review papers by Murakami et al. [5], Hawryluk et al. [6], and Bell et al. [7]. A summary of the best confinement parameters achieved as of May 1986 is given in Table 1 for several modes of plasma operation. Density-confinement time ($n_e(0)\ \tau_E$) products of 10^{20} $m^{-3}s$ have been obtained by pellet fueling. The highest ion temperatures (~ 9 keV) have been achieved with neutral beam injection at low plasma densities. In this "energetic ion regime," a substantial fraction of the core plasma consists of beam-injected ions. The best achieved $n\tau_E T_i$ product of ~ 2 x 10^{19} m^{-3}·s keV has been obtained by pellet injection into ohmically heated plasmas.

Extending the operational limits of TFTR, either at low densities in the energetic ion regime, or with higher density pellet-fueled discharges, will require continued study of plasma-material interactions, specifically the development of a means of plasma density and/or plasma edge-profile control, in addition to the usual requirement of minimizing impurity influx.

2.0 FIRST-WALL CONDITIONING

During the summer of 1985 a significant amount of new first-wall hardware was installed within the TFTR vessel to prepare the device for high power neutral beam operation. The new internal hardware included a full toroidal bumper limiter consisting of 1850 kg of graphite tiles and a full complement (36) of ZrAl surface pumping panels. The considerable increase in graphite surface area (20 m^2) compared to the previously installed moveable limiter (4 m^2) affected the vessel conditioning procedures. The initial conditioning of the vessel with the new internal hardware involved a 6-week period with the vessel heated to 150°C. During this time 130 hours of glow discharge cleaning (GDC) and 175 hours of pulse discharge cleaning (PDC) were applied. Following cooldown of the vessel to ambient temperatures, high power discharge performance was not satisfactory. After a single high current (2.2 MA) disruption, no subsequent high current discharges could be made until the machine was reconditioned by pulse discharge cleaning, followed by an extended series of discharges with increasing plasma current and frequent disruptions at each new current level. When disruptions at the maximum current level (2.5 MA) would not significantly affect the next discharge, the vessel was taken to be in a conditioned state. At this point high current ohmic discharges were characterized by low values of $P_{rad}/P_{OH} < 50\%$ and $Z_{eff} < 1.5$ at $\bar{n}_e > 4.0 \times 10^{19}\ m^{-3}$.

The above conditioning procedure, dubbed "disruptive discharge cleaning" (DDC), was found necessary and was applied in a more systematic fashion following a recent short vessel maintenance period that involved venting the torus to atmosphere for one week (March 3-10). A vessel conditioning regimen of 10 hours of GDC and 60 hours of PDC during a 7-day vessel bakeout at 150°C showed favorable residual gas analysis trends, i.e., impurity (H_2O, CO, CH_4)

production dropped by a factor of 10 during GDC and a factor of 5 during PDC. However, following cooldown of the vessel to ambient temperatures, high power discharge performance was again hindered by excessive outgassing from the bumper limiter. Successful high power discharge operation was attained after a two-day procedure that involved more PDC and a DDC sequence of ~ 100 discharges spanning plasma current levels of 0.6-2.5 MA. The current was increased by 200 kA after a forced disruption at a given plasma current did not affect the succeeding discharge. As this procedure progressed, the radiated power fraction of nondisruptive discharges showed a systematic drop (Fig. 1).

We surmise that the surface heating of the bumper limiter due to the heat load deposited by disruptions is of prime benefit to the limiter conditioning process. Measurements [8] of the surface temperature of the bumper limiter following a 2.2 MA disruption yield temperature rises of $\Delta T \sim$ 1000°C. We calculate that this flash heating will desorb H_2O from a toroidally symmetric area of ~ 10 m^2 and from a depth characteristic of the thermal diffusion length (~ 1 mm). Recent laboratory measurements have shown that the bumper limiter graphite [9] (POCO AXF-5Q) and similar forms of graphite [10] will absorb substantial (~ Torr-l/g) quantities of H_2O following short (< 8 hours) atmospheric exposures. Subsequent thermal desorption measurements [9,10] show that the TFTR 150°C vessel bakeout temperature is ineffective in desorbing the H_2O because the primary desorption temperature for H_2O is in the range of 300-350°C.

Comparing our conditioning experience with the toroidal bumper limiter thus far with the previous conditioning history of the moveable limiter, we note the following differences. Our previously described [2,11] conditioning procedure of vessel bakeout of 150°C concurrent with GDC followed by PDC, was

sufficient to condition both the vessel and the moveable limiter. No significant problems were experienced with regard to recovery from the effects of disruptions. However, a slowly improving plasma impurity situation was observed as a function of exposure of the moveable limiter to high power discharges [11]. Immediately after the initial discharge cleaning period, the fraction of radiated power in standardized ohmic discharges ("fiducials") was ~ 100%. The P_{rad} fraction slowly dropped to < 40% after 2000 discharges. Correlated with this drop were decreases in both carbon and oxygen radiation. A short period (~ 1 week) of atmospheric exposure appeared to have little effect on this long-term conditioning trend.

In contrast, the behavior with the bumper limiter showed that standard vessel conditioning procedures were insufficient to degas the bumper limiter. The above-described procedure of intentional exposure to a series of disruptive discharges at increasing current levels (DDC) was needed for limiter degassing. However, after this procedure, relatively low values of P_{rad} (~ 50-60%) for fiducial discharges were obtained immediately. The long-term conditioning process seen in the case of the moveable limiter was not observed after the initial conditioning of the bumper limiter.

2.1 HYDROGEN-ISOTOPE EXCHANGE

Another conditioning problem related to the porosity of the graphite limiters is the H-isotope exchange process. A previous study by LaMarche et al. [12] has documented the H → D exchange times observed with plasma operation on the moveable limiter. Long exchange times (> 600 discharges for the initial isotopic ratio, $H/(H + D)$, to decay in concentration by 1/e) were observed with the moveable limiter operating at 300°C. With increased power loading during neutral beam injection (NBI), the peak limiter temperature

would rise, and exchange times decreased to ~ 60 discharges for limiter temperatures of 900°C. This behavior is consistent with a thermally activated diffusion process being the rate-limiting step in the exchange process (Fig. 2). An Arrhenius activation energy was determined to be 0.15 eV, an energy characteristic of surface diffusion. To account for the amount of H desorbed from the limiter during the exchange process, a reservoir of bulk hydrogen must be invoked. Therefore, it is possible that the surface diffusion that is relevant to the H-D exchange process includes diffusion along the surface of voids within the bulk graphite which communicate to the surface. Laboratory measurements on samples of the AXF-5Q graphite used for fabrication of the TFTR limiters show evidence of bulk porosity which is connected to the surface. BET [13] surface area measurements yield specific surface areas of 0.29 m^2/g for samples as thick as 1 cm [14]. In addition, H-isotope analysis [15] shows a uniformly distributed bulk concentration of ~ 1% H for samples prior to tokamak exposure, and post-plasma analysis shows a small D concentration (9 ± 4 ppm maximum) which has apparently diffused throughout the bulk of the sample after implantation in the near surface layer.

The H → D exchange times observed thus far with bumper limiter operation are intermediate compared to observations on the moveable limiter. The first H → D exchange with the bumper limiter occurred after the initial conditioning by GDC, PDC, and DDC. The exchange was performed with an extended series of moderate density ($\bar{n}_e$ = 3 x 10^{19} m^{-3}), 2.2 MA, ohmic discharges, and 110 discharges were required for 1/e exchange. This exchange time is consistent with the exchange model described in Ref. 12, with the assumption that ohmic discharges produce negligible heating of the bumper limiter, such that the diffusion of hydrogen to the surface of the limiter is negligible. Thus, incident plasma particles exchange only with a limited volume of graphite

containing absorbed hydrogen. This volume is determined by the bumper limiter scrape-off area times the mean implantation depth. The assumption of negligible surface heating of the bumper limiter for normal ohmic discharges is reasonable. The power loading is sufficiently small (< 13 watts/cm^2) that surface temperatures are below the limit of detectability for the limiter infrared diagnostics [8]. Estimates of the surface temperature rise derived from standard thermal models for graphite yield an upper limit of $\Delta T \sim 25°C$ for a typical 5-sec long, 2.2 MA ohmic discharge. (The bulk temperature does not exceed ~ 50°C.)

2.2 GETTERING STUDIES

Two types of gettering schemes have been studied in TFTR for impurity and plasma density control: (1) a bulk gettering system employing an array of ZrAl pumping panels [3], and (2) an evaporative getter system employing Cr sublimation sources [4]. Tests of the prototype for the ZrAl Surface Pumping System (SPS), which included an array of six ZrAl panels were conducted in 1983/84 [3,16]. The prototype system achieved a pumping speed of 120 m^3/s (for D_2), and improved the residual gas partial pressures over the normal case of pumping with only the torus turbomolecular pumps (with 10 m^3/s). However, no effect of this increased pumping capability was observed on plasma impurity levels or recycling. Recent calculations confirm the null result with respect to recycling control. Using a three-dimensional neutral transport code [17], we calculate that only a small fraction (~ 10^{-3}) of the hydrogen neutrals recycling from the moveable limiter are captured by the pumping panels in the SPS prototype array [18]. The full SPS system consisting of 36 pumping panels was installed in 1985. To date the system has not been tested.

In order to test the difference in gettering schemes between the high pumping speed provided by the SPS system and the high surface coverage provided by the conventional evaporative getter schemes, a series of Cr getter tests were performed during January-April 1985 [4]. These experiments involved evaporating a thin layer (10-100 μm) of Cr over 70% of the TFTR vessel. (The moveable limiter was shielded from direct evaporation.) The first evaporation of Cr within the torus had relatively long lasting effects on both residual gas behavior and subsequent plasma performance: (1) the oxygen radiation was depressed by approximately a factor of two for a period of 3-5 days of plasma operation; (2), the ohmic density limit was increased by 20%; and (3), the partial pressures of oxygen-containing residual gases were depressed by a factor of ten for a period of ~ 10 days. Since the evaporated Cr layer increased the torus pumping speed for active gases only by a factor of two [4], we concluded that the surface coverage effects of the gettering were more important than the increased pumping speed. Evidently, the vessel wall (prior to the installation of the bumper limiter) was an important source of oxygen, and the oxygen introduction mechanism (wall sputtering or desorption) was depressed by overcoating the mixed oxide layer on the vessel surfaces with Cr. The effect of the Cr gettering on the plasma density behavior must be related to the importance of oxygen radiation near the density limit, since an evaporated Cr layer will not pump significant quantities of hydrogen. Further details of the Cr getter experiment are given in Ref. 4, and an expanded discussion of impurity studies in TFTR is given in the next section. With the installation of the toroidal bumper limiter, further use of evaporative Cr gettering in TFTR became impractical, and was discontinued.

3.0 IMPURITY STUDIES

In this section we discuss soft x-ray [19], visible [20], and vacuum-ultraviolet [21] spectroscopic measurements of plasma impurities in ohmically heated and neutral-beam-heated TFTR discharges. The dependence of impurity densities on basic plasma parameters such as the plasma density, current, and fuel gas are described. These measurements are compared to model calculations of limiter and wall sputtering in an attempt to identify the important impurity production mechanisms in TFTR.

3.1 IMPURITY MEASUREMENTS

Figure 3a shows the Z_{eff} variation for a density scan of high current (2.2 MA), ohmic D^+ plasmas for operation on the moveable limiter and on the bumper limiter. The low density limit for this density scan is termed the recycling limit, and is the density which results from a discharge that is fueled only by prefilling the torus with gas sufficient to satisfy breakdown requirements. The high density limit (5-5.5 x 10^{19} m^{-3}) is determined by the onset of disruptions (see Section 4.0). The value of Z_{eff} falls smoothly between these limits reaching ~ 1.2 near the high density limit. These measurements were made with a single channel x-ray pulse-height analysis spectrometer viewing the central chord of the plasma. The measurements were modeled with analytic n_e and T_e profiles chosen to approximate typical Thomson scattering profiles. Reanalysis using measured Thomson scattering profiles increases Z_{eff} values by about 0.2 to 0.4 suggesting a minimum Z_{eff} of ~ 1.5. Z_{eff} values of 2.0 have been obtained at the density limit (n_e = 8.0 x 10^{19} m^{-3}) of He discharges [20]. Spectroscopic analysis [20,21] shows that the low-Z impurities, carbon and oxygen, are the dominant contributors to Z_{eff} and the radiated power. At low densities, $\bar{n}_e$ < 2 x 10^{19} m^{-3}, the low-Z

impurity concentration is of the order of 10% and is primarily carbon with the C/O density ratio ≈ 10. At the density limit, the low-Z impurity concentration falls below 1.5% with approximately equal contributions by carbon and oxygen. Carbon and oxygen densities show opposite trends with electron density indicating that different source mechanisms are operative. The carbon density falls monotonically with $\bar{n}_e$, and the oxygen density rises monotonically with $\bar{n}_e$.

The primary metallic impurities (Fe, Cr, and Ni) are constituents of the stainless steel and Inconel vessel components. The metal concentrations in these ohmic plasmas, shown in Fig. 3b, are negligible, falling exponentially with $\bar{n}_e$ from relative concentrations of $< 4 \times 10^{-4}$ at low densities (2×10^{19} m^{-3}) to $\sim 1 \times 10^{-5}$ at the density limit. The dashed curve shows, for comparison, results obtained while operating on a well-conditioned moveable limiter with the Inconel bellows cover plates still fully exposed to the plasma [19]. The rapid fall-off of metallic impurity concentrations with $\bar{n}_e$ correlates with the edge plasma cooling (and thus decreased sputtering yields) which accompanies increased plasma densities. Furthermore, a trend of increasing metal densities is observed with increased plasma current [19], which heats the edge plasma. Thus, the observed trends with density and current are consistent with a sputtering mechanism as a source for the metallic impurities.

The contribution of the plasma impurities to the radiated power [21] in ohmic discharges is shown as a function of $\bar{n}_e$ in Fig. 4. Here again, the opposing trends of oxygen and carbon and the negligible contribution of the metals are evident. The data points shown in Fig. 4 are based on VUV spectroscopy measurements of various impurity lines and modeling of the impurity transport using the MIST code [22]. The total radiated power

obtained by summing the values from the individual elements agrees (within ± 20%) with the total radiated power measured with bolometers.

The impurity content of neutral-beam-heated discharges in TFTR is illustrated in Fig. 5 as a function of the input power. During the first series of NBI experiments in 1985 operated on the moveable limiter, a rise in Z_{eff} of $\Delta Z \approx 1$ is seen for moderate injected powers ($P_{heat} < 7$ MW). With more recent operation on the bumper limiter, and at higher injected powers (10 MW), there appears to be no significant rise in Z_{eff} with injected power up to 9 MW. The data shown in Fig. 5 are characteristic of a conditioned bumper limiter. Data obtained during NBI experiments earlier in the conditioning cycle (i.e., shortly after an atmospheric exposure) show significant excursions in the low-Z impurity content with NBI. Increases in the metal densities are seen with NBI, but the increased levels do not make significant contributions to Z_{eff} or the radiated power.

3.2 IMPURITY SOURCES

The probable sources for the impurities observed in TFTR discharges can be identified based on a number of general observations. The observed metallic impurities (primarily Fe, Ni, Cr, and Ti) are believed to enter the plasma from sputtering and/or erosion of an equilibrium metal oxide/carbide layer on the graphite limiter surface. This metal oxide/carbide layer builds up as metals are first removed from plasma-exposed sections of the vacuum vessel, and are then redeposited by the scrape-off plasma onto the limiter surface. Evidently, an equilibrium metal layer, which represents a balance of the competing deposition and erosion processes, builds up on the limiter, because very similar results have been obtained from surface analysis of the TFTR limiter tiles removed after the 1983/84 [23] and 1984/85 [24] plasma

operations. Figure 6 shows the results of the most recent surface analysis which was performed during a one-week break in operations in March 1986. The profile of metal deposition across the limiter tiles reflects the competing effects of erosion and deposition. The deposition minimum occurs on the area where the power flux is maximum (Fig. 6). Similar deposition measurements were obtained with the first post-plasma exposure surface analysis of the bumper limiter; deposits of 10^{17}-10^{18} metal atoms/cm^2 are observed over the scrape-off area. Surface analysis of the JET limiter tiles show a remarkably similar pattern [25].

Further evidence that the redeposited metal layer on the limiter surfaces is the primary source of metallic impurities comes from the following two observations: (1) when the moveable limiter was installed in TFTR in 1983, the graphite tiles were coated with a nominally 25 μm TiC layer. During the subsequent operations period the coating partially failed [26], and it was removed prior to the 1984/85 operations period. After removal of the TiC coating the Ti concentration [19] in the plasma decreased by a factor of 50. (2) A recent series of experiments in TFTR has focussed on the formation of detached plasmas [27,28]. After detachment of the plasma from the moveable limiter, the line emission of metallic impurities in the soft x-ray region is attenuated to below the noise level in the spectrometer [28].

With regard to the source of the low-Z impurities, the obvious source of the primary impurity, carbon, is the limiters. No spatially resolved spectroscopic measurements of low ionization states of impurities have been made in TFTR in order to quantify the relative influx rates from the limiter and wall. However, the Cr gettering experiment described in Section 2.2 provided some information on the relative importance of the two sources. The Cr evaporation was applied only to the wall in these experiments and not the

limiter which was shielded from direct evaporation. Since the gettering affected the oxygen but not the carbon impurity content, we conclude that the limiter is the primary source of carbon, but that both the wall and limiter represent potential sources of oxygen accessible to the discharge.

3.3 IMPURITY SCALING WITH FUEL GAS SPECIES

To further investigate the impurity sources and possible mechanisms of impurity generation, the impurity content variation with the fuel gas species was investigated. No significant change was observed in the impurity levels of high current (1.8-2.2 MA) ohmic discharges as the fuel gas was changed from hydrogen to deuterium. With the change from deuterium to ^{4}He, no change was observed in the low-Z impurity content at constant electron density (Fig. 7a). However, the metallic impurity concentrations increased by a factor of 1-2 at low electron density and by a factor of 3-8 at high electron density (Fig. 7b).

If physical sputtering by fuel ions were the dominant impurity generation mechanism, and if impurity transport and plasma edge temperatures were insensitive to the gas species, we would expect large changes in both the carbon and metal impurity content as the gas species is changed from H to D to He. Figure 8 shows laboratory sputtering data [29,30] for various species incident on graphite for the energy range of interest for tokamak edge plasmas. Assuming a simple model [31] for the sheath which develops at the limiter (with secondary emission coefficient, γ_e), ions with charge Z and mass m_i will impact the limiter, with energies E_i equal to

$$E_i = 2kT_i + ZkT_e \ln\left[\frac{m_i}{2\pi m_e}\left(Z + \frac{T_i}{T_e}\right)^{-1}\left(1 - \gamma_e\right)^2\right]^{1/2} \qquad \text{Eq. 1}$$

$$= 3\ ZkT_e + 2\ kT_i \qquad (\text{for } T_i \sim T_e,\ \gamma_e \approx 0)\ ,$$

where T_e and T_i are the edge electron and ion temperatures, respectively. The edge electron temperature for a mid-density (4×10^{19} m^{-3}) ohmic D^+ discharge in TFTR is 75 eV based on Langmuir probe analysis [32], and limiter power loading. Thus fuel ions will impact the limiter at energies near the sputtering curve maximum, 375 eV for H^+ and D^+, and 500 eV for He^{++} incident ions (assuming a constant value for the edge temperature). The sputtering yields at the same electron density are in the ratio of $\leq$ 5:2.7:1 for He/D/H, respectively. These yields cannot be directly compared to the relative impurity density measurements in TFTR because of the unknown edge transport properties of the different fuel species. However, if one assumes that the impurity confinement times are similar in H, D, or He plasmas (and such similarity has been measured for Si transport in H or D discharges in ASDEX [33]), then physical sputtering alone cannot account for the observed small variation in carbon density in TFTR with fuel species.

A more sophisticated calculation of physical sputtering was made using the three-dimensional neutral transport code DEGAS [17], which calculates the integrated sputtered flux due to physical sputtering by the intercepted ion flux on the moveable limiter and the charge-exchange flux on the limiter. The geometry of the scrape-off area on the moveable limiter was divided into 7 segments according to the range of ion flux [34]. Figure 9 shows the results of this calculation assuming physical sputtering coefficients for three types of limiter surfaces: (1) pure graphite, (2) a metal carbide, and (3) a characteristic medium-Z metal (V). These three types of materials span the probable surface composition of the moveable limiter. Sputtering measurements on samples taken from plasma-exposed TFTR moveable limiter tiles [35] show

that the sputtering coefficient is characteristic of pure graphite in the center of the scrape-off area where the incident particle range is larger than the metal deposition layer. On the edge of the tile where metal deposition is thicker, the tile has a sputtering coefficient characteristic of a metal. The Fig. 9 results show that physical sputtering by charge exchange neutrals is small in comparison to physical sputtering by fuel ions, and show again the large variation in ion sputtering with gas species for all three types of surfaces.

Two other sputtering mechanisms to be considered are chemical erosion and impurity ion sputtering. Adding the chemically eroded CH_4, using the data of Roth [36], results in a smaller variation in impurity sputtering yields of carbon (at the same electron density) with ratios of 5.5:4:3 from He^{++}, D^+, and H^+, respectively. The dependence of sputtering on fuel ion is now weaker.

A source mechanism for carbon which is probably active at the lower plasma densities is impurity ion (O^{+n}, C^{+m}) sputtering, based on the modest impurity scaling with species and the sputtering data in Fig. 8. Ramsey et al. [20] have attempted to match the shape of the observed carbon density as a function of edge temperature with the sputtering data of Fig. 9. Except for the lowest edge temperatures (i.e., highest edge densities) significant contributions of self-sputtering and oxygen sputtering are needed to match the energy dependence of carbon impurity density. In addition, Ramsey et al. [20] find that the effective sheath potential must be lowered by a factor of ~ 2 over the value given in Eq. 1. This is consistent with the recent observations made on DITE [37] which indicate that the sheath potential on carbon surfaces is lower than ~ 3 kT_e because of the effects of secondary electron emission.

4.0 PLASMA FUELING AND RECYCLING

TFTR discharges are fueled by standard gas injection techniques or by a combination of gas fueling with neutral beam or pellet injection. This section reviews the fueling characteristics and the differences in recycling behavior that are observed for these three fueling techniques.

4.1 GAS FUELING

Gas input is required only during the current and density rise portions of the TFTR discharge cycle. No gas input is required to maintain steady-state densities for the 3-5 second period of constant current. This behavior is characteristic of the entire density range accessible by gas fueling, (1-5.5) x 10^{19} m^{-3}, and is attributed to the combined effect of long particle confinement times and efficient recycling (R ≈ 1).

In general, a small difference in the required gas input is noted between operation on the moveable-limiter (Fig. 10a) versus operation on the toroidally symmetric bumper-limiter (Fig. 10b). Figure 11 shows the total gas input required to fuel ohmic plasmas for the two limiter configurations as a function of the line-averaged density. The required gas input scales linearly with density, and inversely with the plasma current (not shown). This behavior reflects a trend of decreasing particle confinement time with density and increasing particle confinement time with plasma current, which are also deduced from analysis of H_α emission data [38]. The fueling data shown in Fig. 11 are scattered at low densities (near the recycling limit) where shot-to-shot variations in wall effects (recycling rates) can have large effects on the required gas input. At higher densities approximately 30% more gas is required for bumper-limiter operation than for moveable-limiter operation. A

similar effect was observed in the comparison of gas-fueled rail-limiter versus bumper-limiter discharges in the PDX device [39]. There appears to be no significant difference in plasma confinement with the two limiter configurations [7]. Therefore, the increased gas input requirement must reflect a small decrease in recycling due to the differing plasma-limiter geometry. This geometric difference also affects the evolution of the edge neutral density. With the moveable limiter configuration, the edge neutral pressure (density) during a discharge was below the limit of detection, $\leq 1 \times 10^{-7}$ Torr (3×10^{15} m^{-3}) of ionization gauges located at the torus boundary (LaMarche et al. [40]) regardless of the fueling method (gas, pellets, or neutral beam injection). Recent operation with the bumper limiter also shows edge neutral pressures below 10^{-7} Torr for standard gas-fueled ohmic discharges. However, during neutral beam or pellet injection, and during any of the plasma scenarios that force detachment of the plasma from limiter contact [27], edge neutral pressures (densities) in the range of $(1-3) \times 10^{-7}$ Torr [$(0.3-1.0) \times 10^{16}$ m^{-3}] are detected. The observation of large edge neutral pressures with operation on a toroidally symmetric bumper limiter was also seen in PDX [39]. The effect is attributed to a symmetrization of the recycling flux, which is highly localized in the case of a single poloidal limiter and toroidally symmetric with a bumper limiter.

No significant difference is observed in the fueling curves (Fig. 11) between H-fueled or D-fueled discharges. A similar lack of isotopic dependence was observed in the recycling flux from H_α emission analysis [38]. In contrast to the hydrogen isotope behavior, gas fueling with He is more efficient and attains approximately twice the electron density limit (but the same ion density limit) as hydrogen- (or deuterium) -fueled ohmic discharges.

Since these discharges required no steady-state gas input, the usual definitions of fueling efficiency [39,41,42] are not applicable. For the purpose of discussion of TFTR data, we define the curve of 100% efficient fueling as the line equating the total number of plasma electrons at steady state ($N_e = \int n_e \cdot dV$) to the total input of electrons from gas fueling (i.e., assuming two electrons per input H_2 or D_2 molecule or He atom). With this definition of 100% fueling, an incremental fueling efficiency can be defined equal to the slope dN_e/dN_g where N_g is the number of input electrons. With this definition the fueling efficiency of He discharges is ~ 60% and the efficiency of H- or D-fueled discharges is ~ 20%.

Another indication that the gas fueling efficiency is dependent on the plasma limiter geometry comes from examination of the plasma minor radius scaling of the required gas input. For plasmas with radii < 0.60 m the gas input scales with the plasma volume (~ $R\ a^2$). For the larger plasmas, less than a volume-scaled input of gas is required, presumably because the recycling is more efficient (R closer to unity) in the large plasma geometry.

4.2 NEUTRAL BEAM FUELING

The initial density rise at the onset of NBI corresponds to all beam particles being ionized as shown in Fig. 12b for a typical case. However, later in the beam pulse, the rate of density rise decreases and the density often reaches a constant level (a phenomena known as density clamping). Thus, fueling curves as shown in Fig. 12a show less than 100% fueling efficiency. This behavior is interpreted as a reduction in recycling with increasing beam power. The results of Shimada et al. [38] show that the particle confinement time, τ_p, in TFTR is a function of I_p and n_e, but independent of beam power. For the data shown in Fig. 12a, the current and final density were the same

for all the analyzed discharges, hence the value of τ_p was also the same. Therefore, the density clamps as a result of a decrease in the effective confinement time, $\tau_p^* = \tau_p/(1-R)$, because the value of the recycling coefficient, R, decreases with increasing beam power. This interpretation is further supported by the rate of density decay after NBI. Assuming that the conditions which brought about the reduction in R do not revert to ohmic values too rapidly, the recycling coefficient should remain approximately constant for some time ($\sim \tau_p^*$) after beam turnoff. This is indeed the case, as the density pump-out rate after NBI is only slightly less than the pumping rate required to maintain constant density during NBI (Fig. 12b).

4.3 PELLET FUELING

Pellet fueling experiments [43,44] have been performed in TFTR with two sizes of deuterium pellets, 4 mm and 2.67 mm. Figure 13 shows the plasma density behavior during fueling with a single 4 mm pellet (Fig. 13a), and with three 2.67 mm pellets (Fig. 13b). The fueling efficiency for pellet fueling is generally close to 100% (with some pellet-to-pellet variations) as can be seen from the comparison of the observed density excursions in Fig. 13 with the density rise predicted for 100% conversion of the pellet fuel to plasma electrons. The time constants ($\tau_p^* = 2$-4 s) observed for the density decay following the pellet injection are intermediate in time scale to the short values of τ_p^* (< 1 s) observed with NBI and the long values of τ_p^* (> 10 s) observed for gas fueling.

4.4 RECYCLING

It is interesting to speculate on the observed differences in recycling behavior for gas, pellet, and NBI-fueled discharges. The usual particle

balance equation can be written in which the time derivative of the number of electrons stored in the plasma volume $\dot{N}_e$, is equated to the electron loss rate plus the gas (S_g), neutral beam (S_n), pellet (S_p), and impurity (Z_z) source terms:

$$\dot{N}_e = \frac{-N_e}{\tau_p} + R\frac{N_e}{\tau_p} + S_g + S_n + S_p + S_z \,, \qquad \text{Eq. 2}$$

$$\text{where } \tau_p^* = \tau_p/1-R \approx \frac{N_e}{S_g + S_n + S_p + S_z - \dot{N}_e} \qquad \text{Eq. 3}$$

is the time constant of the density decay when the fueling source terms are zero.

The observed values of τ_p^* in most gas-fueled discharges are greater than 10 s. Using values of τ_p derived from H_α emission and Langmuir probe measurements [38], the recycling coefficient is calculated to be close to unity for gas-fueled discharges.

As noted in Section 4.1, small variations were observed in the gas-fueling measurements depending on the plasma-limiter geometry, such as during the plasma-size scaling experiments, and the moveable/bumper limiter comparison. The only large change in recycling with gas fueling was observed following a recent conditioning experiment with the bumper limiter. After exposing the bumper limiter to a series of low density He discharges, a density decay constant of $\tau_p^* = 2.0$ s was observed for the first high density deuterium discharge that was attempted (Fig. 10c). The effect showed signs of saturation over the succeeding 5 discharges as the required gas input decreased, and the value of τ_p^* increased. We ascribe the observed large drop in τ_p^* to pumping of the edge plasma by the bumper limiter, which effectively decreases the recycling coefficient.

Because of the high level of hydrogen retention (~ 30 atomic %), and the high porosity of POCO graphite, a degassed area of the limiter should act as a transient pump. Calculations of the hydrogenic flux incident on the moveable limiter for a typical ohmic discharge [33] indicate that the relatively small active area (< 0.5 m^2) should saturate in < 0.5 s. Thus the pumping effect would not be observable for most of the discharge period. With the much larger active area of the bumper limiter (~ 10 m^2), the pumping effect should be observable for many discharges if the hydrogen density in the near-surface region (~ 10 nm) is below the saturation density. For the case shown in Fig. 10c, the reduction in τ_p^* to 2.0 s corresponds to a reduction in recycling from R = 1 to R = 0.97, if we assume τ_p = 0.07 s as inferred from H_α measurements [38] of discharges with the same I_p and n_e.

Pumping effects with decreased recycling have also been observed with the large area bumper limiters in JET [45]. However, unlike TFTR, the limiter pumping effects in JET are observed whenever the discharge is brought into contact with the bumper limiter, and does not show signs of saturation. It is not obvious that the difference in wall temperature between JET (at 300°C) and TFTR (at 20°C) can account for different limiter pumping behavior, since neither the bulk diffusivity [46] nor the hydrogenic outgassing [9] is significantly enhanced at 300°C in graphite.

We interpret the observation of smaller values of τ_p^* with NBI and pellet fueling to be a consequence of R being less than unity. Quantitative values of R have been obtained for a series of NBI discharges using Eq. 2 (where in this case the S_n term dominates), and values of τ_p are derived from Langmuir probe and H_α emission measurements [38]. The results of this analysis for a beam pulse such as shown in Fig. 12b show that R drops to ~ 0.8 during the beam injection, and then eventually recovers to R = 1 after termination of the

pulse. This behavior is not unexpected and has been documented in an earlier study in the JFT-2 tokamak [47]. It is likely that R depends on the neutral-beam-injected power because as the injected power increases, both the edge temperature and the mean energy of the charge-exchange flux to the wall will increase. Both effects will lead to decreased recycling, since (1) increasing the plasma edge temperature will lead to increased retention of the ion flux on the limiter, thus decreasing R at the limiter (at least for a transient period until a new saturation limit is reached), (2) and increasing the charge exchange energy will decrease R at the wall. We have not yet studied the variation of R during pellet fueling, however, we suspect that the observed decreased values of τ_p^* can also be ascribed to decreases in R via pellet-induced modification of the plasma edge profile.

5.0 SUMMARY

We have reviewed our studies of plasma-material interactions in TFTR with high current ($\lesssim$ 2.2 MA), ohmically heated and high power (10 MW), neutral-beam-heated discharges. The effects of the two limiter configurations in TFTR, a poloidal moveable limiter, and a toroidal bumper limiter, have been investigated. Conditioning procedures involving various forms of discharge cleaning have resulted in values of $Z_{eff} \lesssim 1.5$ for $n_e > 5 \times 10^{19}$ m^{-3} for ohmic plasmas. Only modest increases in Z_{eff} ($\sim$ 1) have been observed for 10 MW of D° neutral injection. The dominant plasma impurity in terms of contributions to Z_{eff} and plasma radiation is carbon, except near the ohmic density limit where both oxygen and carbon are comparable. Metallic impurities from vacuum vessel metals (Fe, Cr, Ni, and Ti) are negligible in terms of contributions to Z_{eff} or plasma radiation. The conditioning time, either for reducing the low-Z (C, O) impurity influx from the limiter following an atmospheric vent, or

for isotopic exchange (H + D) apparently is driven by the high porosity of the limiter material (AXF-5Q graphite). The dominant source of impurities appears to be ion sputtering of the limiter, except for oxygen for which (sputtering or desorption from) the wall may represent an equally important source. The dominant sputtering process for carbon is unknown.

A recycling coefficient near unity and large values of the effective particle containment time ($\tau_p^* > 10$ s) have been observed for most gas-fueled discharges. Gas-fueled discharges with $R < 1$ have been observed after helium discharge conditioning of the bumper limiter so that it pumps during a subsequent deuterium discharge. Discharges fueled by neutral beam or pellet injection routinely show lower values of τ_p^* and recycling less than unity. Future plasma material interaction studies in TFTR will most likely concentrate on additional means of plasma density control via control of plasma recycling. Density control is important for the optimization of H, D, and T isotopic ratios and density profiles for NBI and ICRF heating experiments.

ACKNOWLEDGEMENTS

We acknowledge the efforts and technical skills of the TFTR Facility Operations and Neutral Beam operations groups, and thank H.P. Furth, P.H. Rutherford, D.J. Grove, and J.R. Thompson for their support and encouragement. This work was performed under US DOE Contract No. DE-AC02-76-CH03073.

REFERENCES

[1] H.F. Dylla, W.R. Blanchard, R.J. Hawryluk, et al., J. Nucl. Mater. 128/129 (1984) 861.

[2] H.F. Dylla, W.R. Blanchard, R.B. Krawchuk, R.J. Hawryluk, and D.K. Owens, J. Vac. Sci. Technol. A2 (1984) 1188.

[3] J.L. Cecchi, M.G. Bell, M. Bitter, et al., J. Nucl. Mater. 128/129 (1984) 1.

[4] H.F. Dylla, P.H. LaMarche, W.R. Blanchard, et al., J. Vac. Sci. Technol. A4 (1986) 1753.

[5] M. Murakami, V. Arunasalam, J.D. Bell, et al., Proc. 12th European Conf. on Controlled Fusion and Plasma Physics, (Budapest, Hungary) 2-6 September 1985, Plasma Physics and Controlled Fusion 28 No. 1A (January 1986) pp. 17-27.

[6] R.J. Hawryluk, V. Arunasalam, M.G. Bell, et al., Proc. of the Royal Society Symposium on the JET Project and the Prospects for Controlled Fusion, London, 1986 (to be published in Proc. Royal Soc.).

[7] M.G. Bell, V. Arunasalam, M. Bitter, et al., Proc. 13th European Conf. on Controlled Fusion and Plasma Physics, (Schliersee, West Germany) 14-18 April 1986.

[8] M. Ulrickson and S.S. Medley, (to be published in J. Nucl. Mater.).

[9] A.E. Pontau and D.H. Morse, Proc. 2nd Intern. Conf. on Fusion Reactor Materials, Chicago 1986, (to be published in J. Nucl. Mater.).

[10] J. Bohdansky, C.D. Croesmann, J. Linke, et al., Proc. Workshop on Surface Modification by Plasma Surface Interactions, Princeton 1986, (to be published in Nucl. Instr. Methods).

[11] P.H. LaMarche, H.F. Dylla, F.P. Boody, et al., (to be published in J. Nucl. Mater.).

[12] P.H. LaMarche, H.F. Dylla, P.J. McCarthy, and M. Ulrickson, J. Vac. Sci. Technol. A4 (1986) 1198.

[13] S. Brunauer, P.H. Emmett, and E. Teller, J. Am. Chem. Soc. 60 (1938) 309.

[14] R. Bastasz, S. Fukuda and Y. Yamashina, unpublished results.

[15] W.R. Wampler, B.L. Doyle, and A.E. Pontau, (to be published in J. Nucl. Mater.).

[16] J.L. Cecchi, P.H. LaMarche, H.F. Dylla, and R.J. Knize, J. Vac. Sci. Technol. A3 (1985) 487.

[17] D.B. Heifetz et al., J. Comput. Phys. 46 (1982) 309.

[18] D.B. Heifetz, in Physics of Plasma-Wall Interactions in Controlled Fusion, D.E. Post, R. Behrisch, eds. (Plenum, New York, 1986) pp. 695-772.

[19] K.W. Hill, M. Bitter, N.L. Bretz, et al., Nucl. Fusion (in press).

[20] A.T. Ramsey, K.W. Hill, F.P. Boody, et al., (to be published in J. Nucl. Mater.).

[21] B.C. Stratton, A.T. Ramsey, R.J. Groebner, et al., unpublished results.

[22] R.A. Hulse, Nucl. Technol./Fusion 3 (1983) 259.

[23] H.F. Dylla, M.A. Ulrickson, P.H. LaMarche, D.K. Owens, and B.L. Doyle, J. Vac. Sci. Technol. A3 (1985) 1105.

[24] A.E. Pontau, W.R. Wampler, B.E. Mills, et al., J. Vac. Sci. Technol. A4 (1986) 1193.

[25] J. Ehrenberg, R. Behrisch, P. Martinelli, et al. Controlled Fusion and Plasma Physics, Vol. 9F, Pt. II (1985) 535.

[26] M. Ulrickson, J.L. Cecchi, B.L. Doyle, H.F. Dylla, S.S. Medley, D.K. Owens, and P. Trester, J. Nucl. Mater. 133/134 (1985) 253.

[27] J.D. Strachan et al. Proc 12th European Conf. on Controlled Fusion and Plasma Physics, (Budapest, Hungary 1985) J. Fusion Technology 8 No. 1, Part A, 339 (July 1986)

[28] J.D. Strachan, F.P. Boody, C. Bush et al., (to be published in J. Nucl. Mater.).

[29] J. Roth, J. Bohdansky, and W. Ottenberger, Report IPP 9/26 (May, 1979) Max-Planck-Institut fur Plasmaphysik, Garching.

[30] E. Hechtl, J. Bohdansky, and J. Roth, J. Nucl. Mater. 103/104 (1981) 333.

[31] P.C. Stangeby in Physics of Plasma-Wall Interactions in Controlled Fusion, D.E. Post and R. Behrisch, eds. (Plenum, New York, 1986) pp. 41-98.

[32] R. Budny, D. Manos, D.K. Owens et al., (to be published in J. Nucl. Mater.).

[33] K. Behringer, G. Fussmann, W. Poschenrieder, et al. Proc. 11th European Conf. on Contr. Fusion and Plasma Physics. (Aachen, 1983) II, p. 467.

[34] D.B. Heifetz, H.F. Dylla, M. Ulrickson, and M.I. Baskes, (to be published in J. Nucl. Mater.).

[35] A.E. Pontau, R.A. Causey, and J. Bohdansky, (to be published in J. Nucl. Mater.).

[36] J. Roth in Physics of Plasma-Wall Interactions in Controlled Fusion, D.E. Post and R. Behrisch, eds. (Plenum, New York, 1986) pp. 389-412.

[37] G.F. Matthews and G.M. McCracken, (to be published in J. Nucl. Mater.).

[38] M. Shimada, A.T. Ramsey, D.K. Owens et al., (to be published in J. Nucl. Mater.).

[39] H.F. Dylla, W.R. Blanchard, R. Budny, R.J. Fonck, D.K. Owens, and G.L. Schmidt, J. Nucl. Mater. 111/112 (1982) 211.

[40] P.H. LaMarche, H.F. Dylla, D.K. Owens et al., Rev. Sci. Instrum. 56 (1985) 981.

[41] TFR Group, J. Nucl. Mater. 93/94 (1980) 272.

[42] H.M. Mayer, F. Wagner, G. Becker, et al., J. Nucl. Mater. 111/112 (1982) 204.

[43] S.L. Milora, G.L. Schmidt, V. Arunasalam, et al., Proc 13th European Conference on Controlled Fusion and Plasma Physics (Schliersee, West Germany) 14-18 April 1986.

[44] G.L. Schmidt et al., in Proc. 12th European Conference on Controlled Fusion and Plasma Physics, 2-6 September 1985 (Budapest, Hungary) Controlled Fusion and Plasma Physics, eds. L. Pocs, A. Montvai, Vol. 9F, Part 2 (September 1985) pp. 674-677.

[45] L. deKock et al., (to be published in J. Nucl. Mater.).

[46] R.A. Causey, M.I. Baskes, and K.L. Wilson, J. Vac. Sci. Technol. A4 (1986) 1189.

[47] H. Matsumoto, H. Kimura, S. Sengoku, N. Suzuki, K. Ohasa, Y. Yamamoto, Nucl. Fusion 22 (1982) 840.

TABLE 1: SUMMARY OF TFTR HEATING AND CONFINEMENT EXPERIMENTS

Regime	I_p (MA)	$\bar{n}_e$ ($10^{19} m^3$)	$n_e(0)$ ($10^{19} m^3$)	τ_E (s)	T_i (keV)	T_e (keV)
Gas Fueled (ohmic)	2.2	5.4	7.2	0.4	~2.3	2.3
Pellet Fueled (ohmic)	1.6	14	28	0.5	~1.4	1.4
Standard NBI (10.4 MW)	1.4	3.0	4.7	0.1	10.5±1	5.2
Pellet Fueled (NBI)	2.2	7.1	11	0.2	~2.3	2.3
Energetic Ion	0.8	1-2	~3	0.1-0.15	9±2	4.6

FIGURE CAPTIONS

Fig. 1 Plasma current and radiated power fraction vs. discharge number during Disruption Discharge Cleaning (DDC) procedure.

Fig. 2 Arrhenius plot of the number of discharges (s_o) required to exchange from H to D as a function of the moveable limiter temperature (from [12] with permission).

Fig. 3 (a) Z_{eff} vs. line-average density ($\bar{n}_e$) for high current (2.2 MA), large radius (a = 0.82 m) ohmic discharges. (b) relative metal concentrations vs. n_e for the same ohmic density scan as plotted in (a). The measurements were derived from pulse height analysis of soft x-ray emission.

Fig. 4 Radiated power due to carbon, oxygen, and metallic impurities as a function of line-averaged plasma density ($\bar{n}_e$) for high current (2.2 MA), large radius (a = 0.82 m) ohmic discharges. The total radiated power, equal to the summation of the individual impurity fractions, agrees with the total power as measured by bolometry [21].

Fig. 5 Z_{eff} vs. neutral beam input power (P_{heat}) for high current (2.2 MA) discharges on the moveable limiter (a), and for the first power scan on the conditioned bumper limiter (b).

Fig. 6 Measured distribution of deposited metals on two of the moveable limiter tiles. The minimum in the deposition distribution corresponds to the region of highest heat flux.

Fig. 7 Comparison of the impurity content of deuterium- and helium-fueled discharges (I_p = 1.8 MA, a = 0.82 m) on the moveable limiter. (a) Z_{eff} vs. line-averaged density ($\bar{n}_e$) derived from visible bremsstrahlung measurements. (b) Relative concentration of Ni vs. $\bar{n}_e$ derived from pulse height analysis of soft x-ray emission.

Fig. 8 Sputtering coefficient as a function of incident particle energy for graphite. The curves for H, D, and He sputtering are from [29], and the curves for C and O sputtering are from [30].

Fig. 9 Calculated sputtered flux from the moveable limiter for a moderate density ($\bar{n}_e = 3.0 \times 10^{19}$ m^{-3}) ohmic discharge, assuming a fuel current of 1×10^{22} particles/sec for H and D discharges and half this value for He discharges. The sputtered flux is calculated for the three fuel ions (H, D, and He) and for three limiter surfaces: pure C, a pure metal (V), and a metal carbide (TiC).

Fig. 10 Gas-fueling and plasma density waveforms for three representative cases in TFTR: typical gas fueling with ohmic discharges on the moveable limiter (a), and bumper limiter (b). The special case of fueling on the bumper limiter, which shows density pumpout (c), was obtained after conditioning with He discharges.

Fig. 11 Gas-fueling curves for ohmic discharges on the moveable and bumper limiters. For comparison the curve of 100% fueling efficiency is drawn assuming the gas input is equal to the volume-integrated plasma density.

Fig. 12 (a) The fueling efficiency of neutral beam injection as a function of the injected power and plasma current. (b) The plasma density behavior during a 0.5 s, 10.5 MW neutral beam pulse into a 1.4 MA discharge.

Fig. 13 The plasma density behavior after injection of one 4 mm deuterium pellet (a) and after the injection of three 2.67 mm deuterium pellets. The density rise equivalent to 100% fueling efficiency for each pellet is noted.

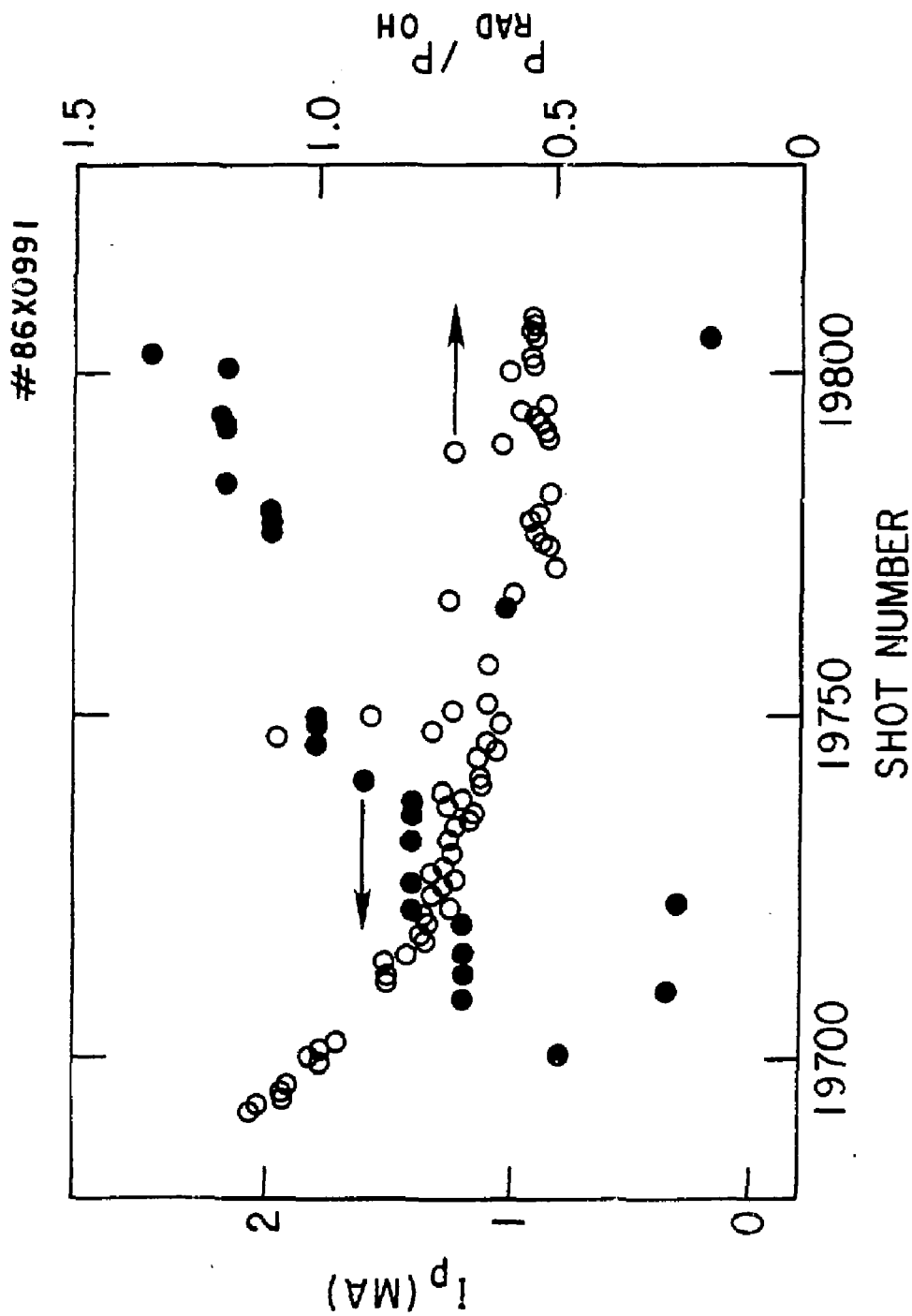
#86X0991
1.5
1.0
0.5
0
P_{RAD}/P_{OH}
2
1
0
I_p (MA)
19700
19750
19800
SHOT NUMBER

Fig. 1

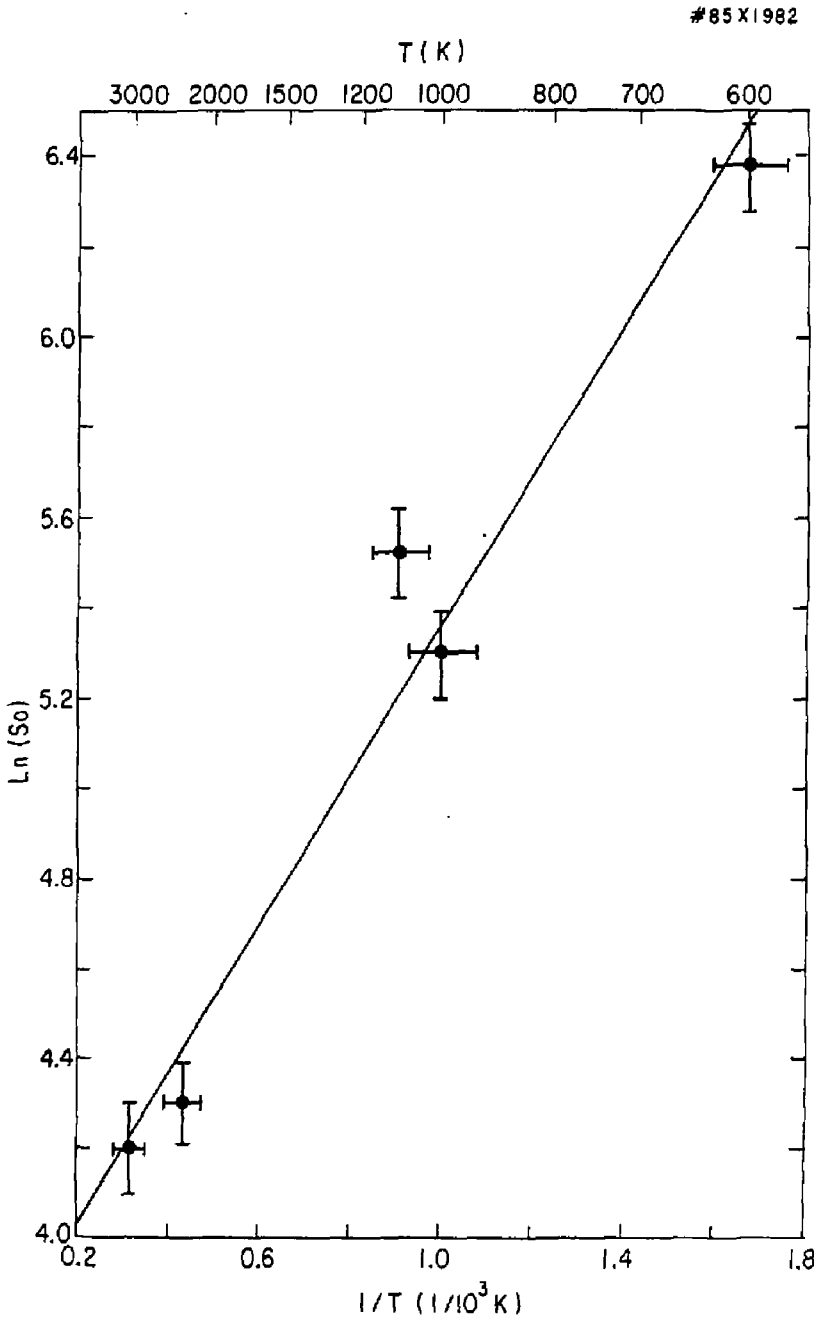
#85X1982
T(K)
3000 2000 1500 1200 1000 800 700 600
6.4
6.0
5.6
5.2
4.8
4.4
4.0
Ln (So)
0.2 0.6 1.0 1.4 1.8
1/T (1/10³K)

Fig. 2

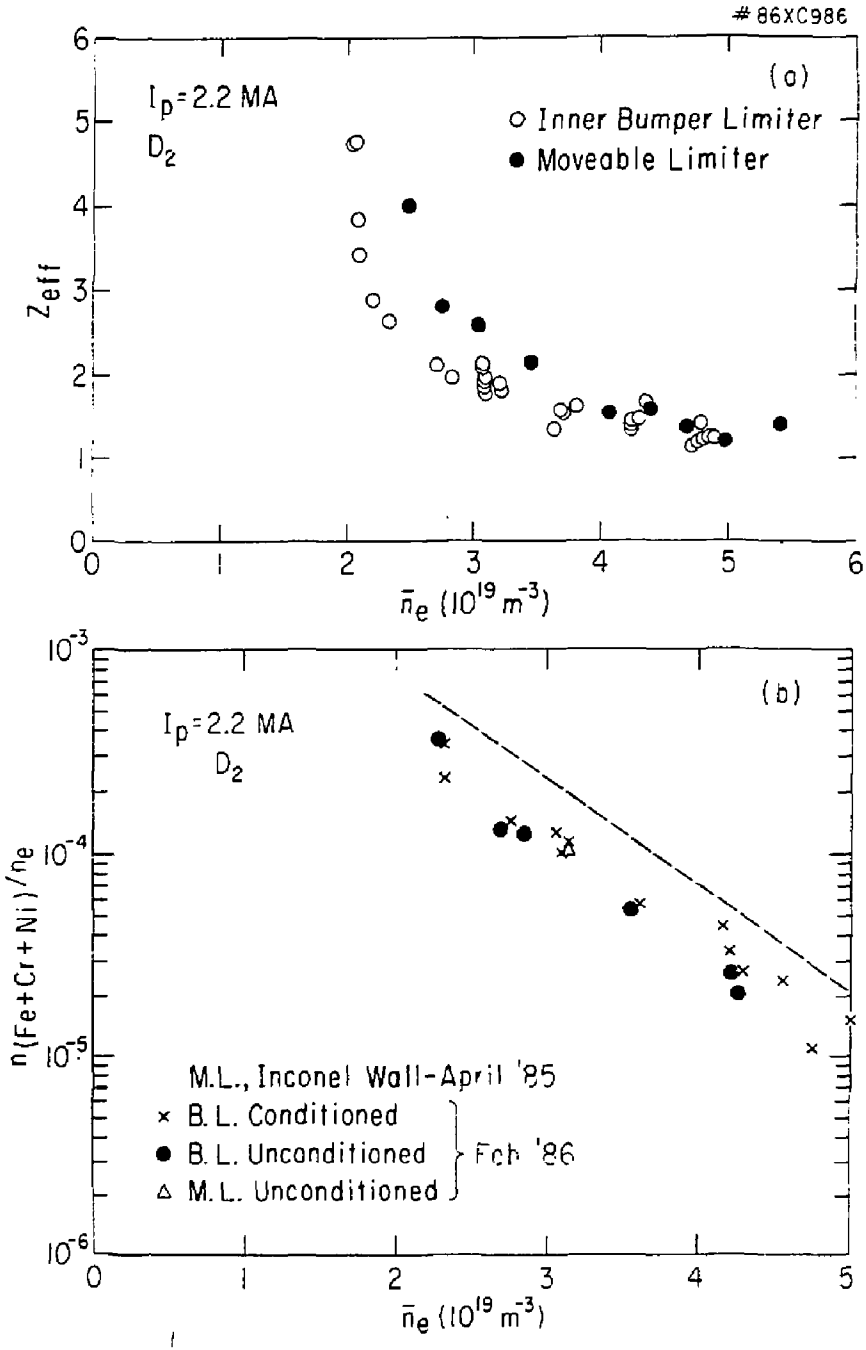
#86XC986
(a)
I_p=2.2 MA
D_2
○ Inner Bumper Limiter
● Moveable Limiter
Z_{eff}
$\bar{n}_e$ (10^{19} m^{-3})
(b)
I_p=2.2 MA
D_2
$n_{(Fe+Cr+Ni)}/n_e$
M.L., Inconel Wall-April '85
× B. L. Conditioned
● B. L. Unconditioned
△ M. L. Unconditioned
} Feb '86
$\bar{n}_e$ (10^{19} m^{-3})

Fig. 3

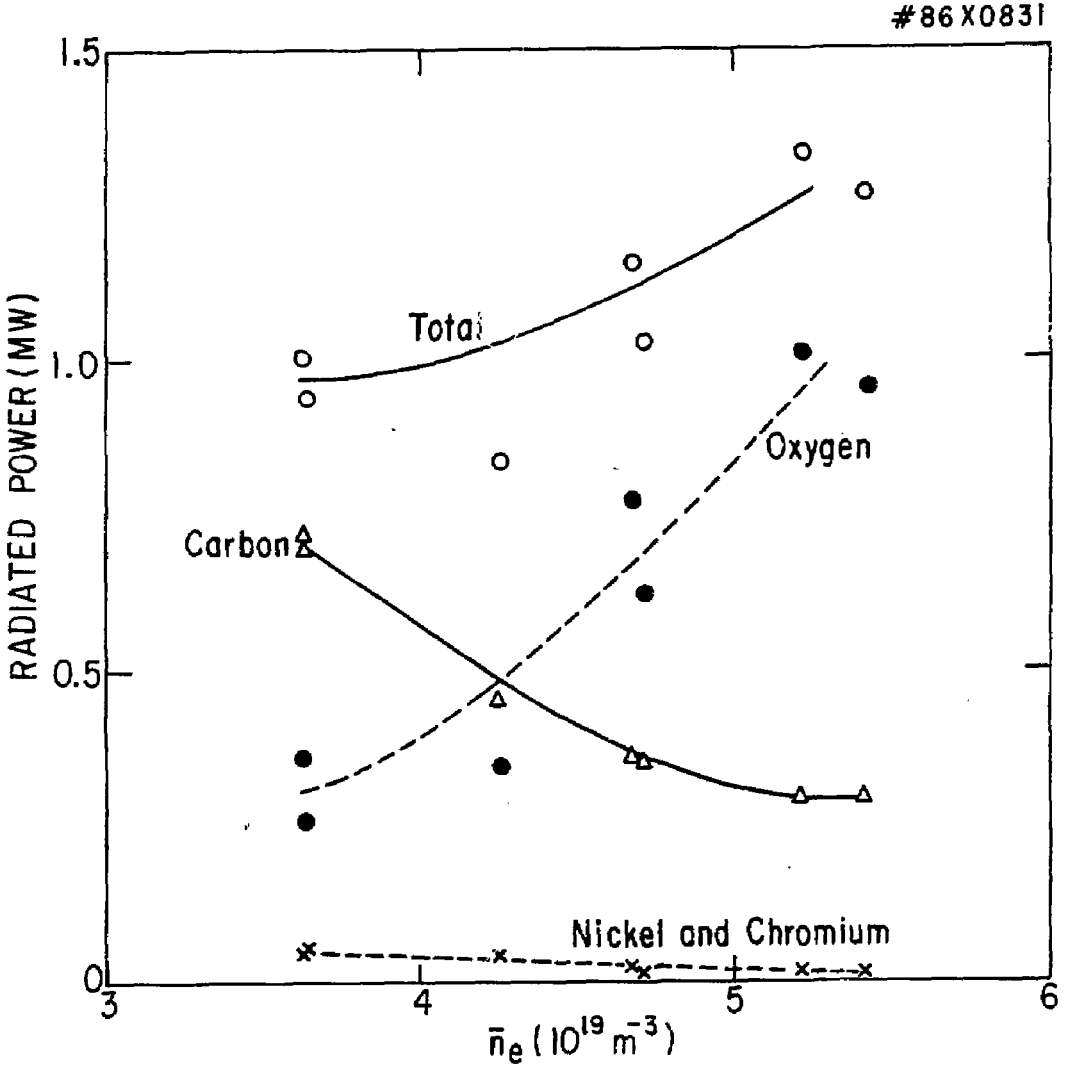
#86X0831
1.5
1.0
0.5
0
RADIATED POWER (MW)
Total
Oxygen
Carbon
Nickel and Chromium
3
4
5
6
$\bar{n}_e$ (10^{19} m^{-3})

Fig. 4

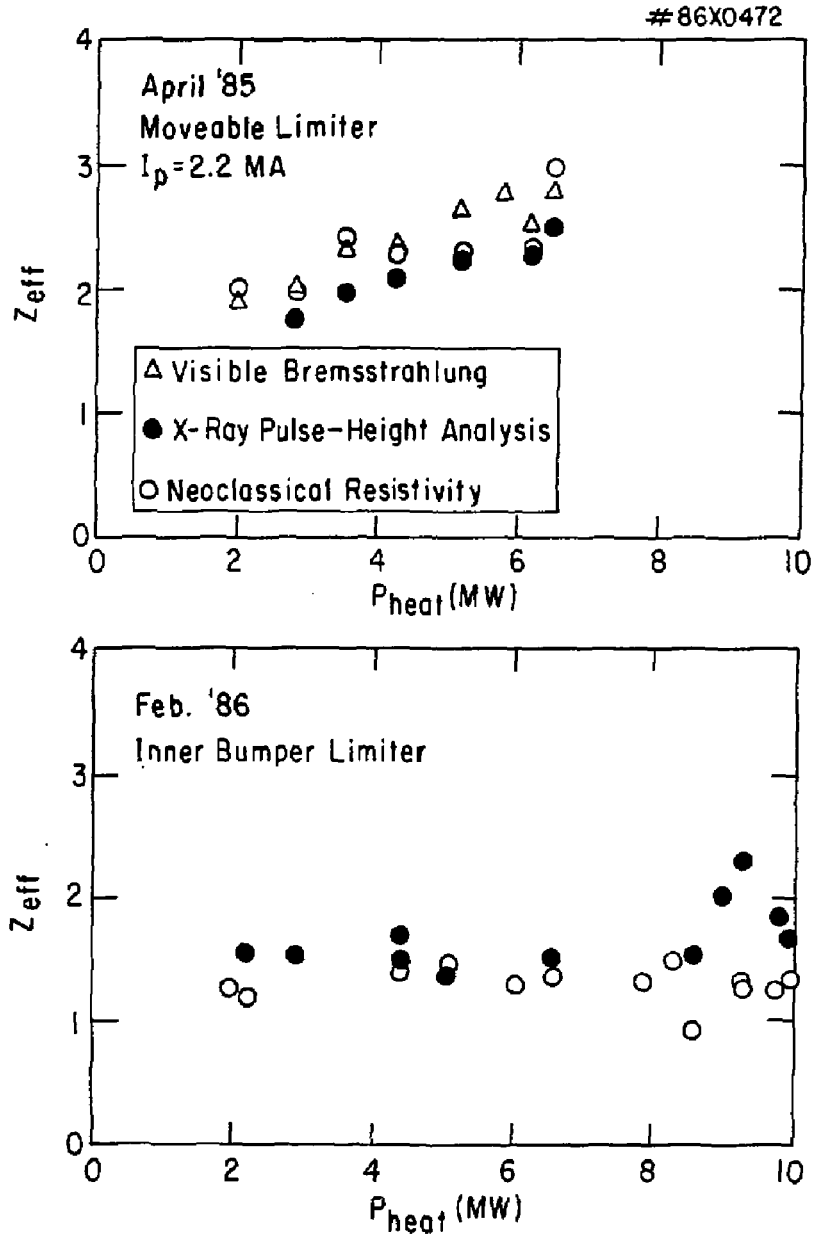
#86X0472
April '85
Moveable Limiter
I_p=2.2 MA
Visible Bremsstrahlung
X-Ray Pulse-Height Analysis
Neoclassical Resistivity
Z_{eff}
P_{heat}(MW)
Feb. '86
Inner Bumper Limiter
Z_{eff}
P_{heat} (MW)

Fig. 5

#86X0854

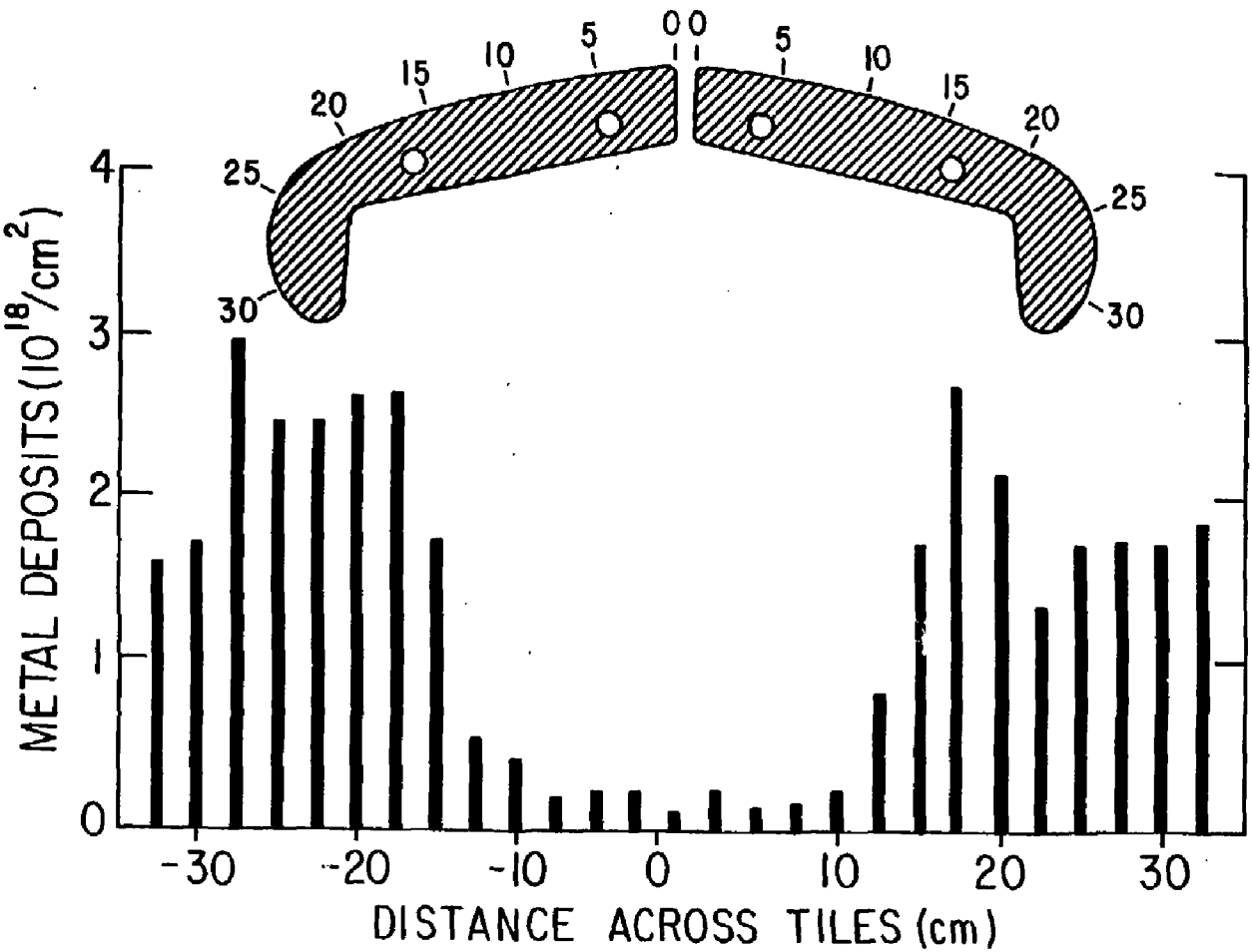

Fig. 6

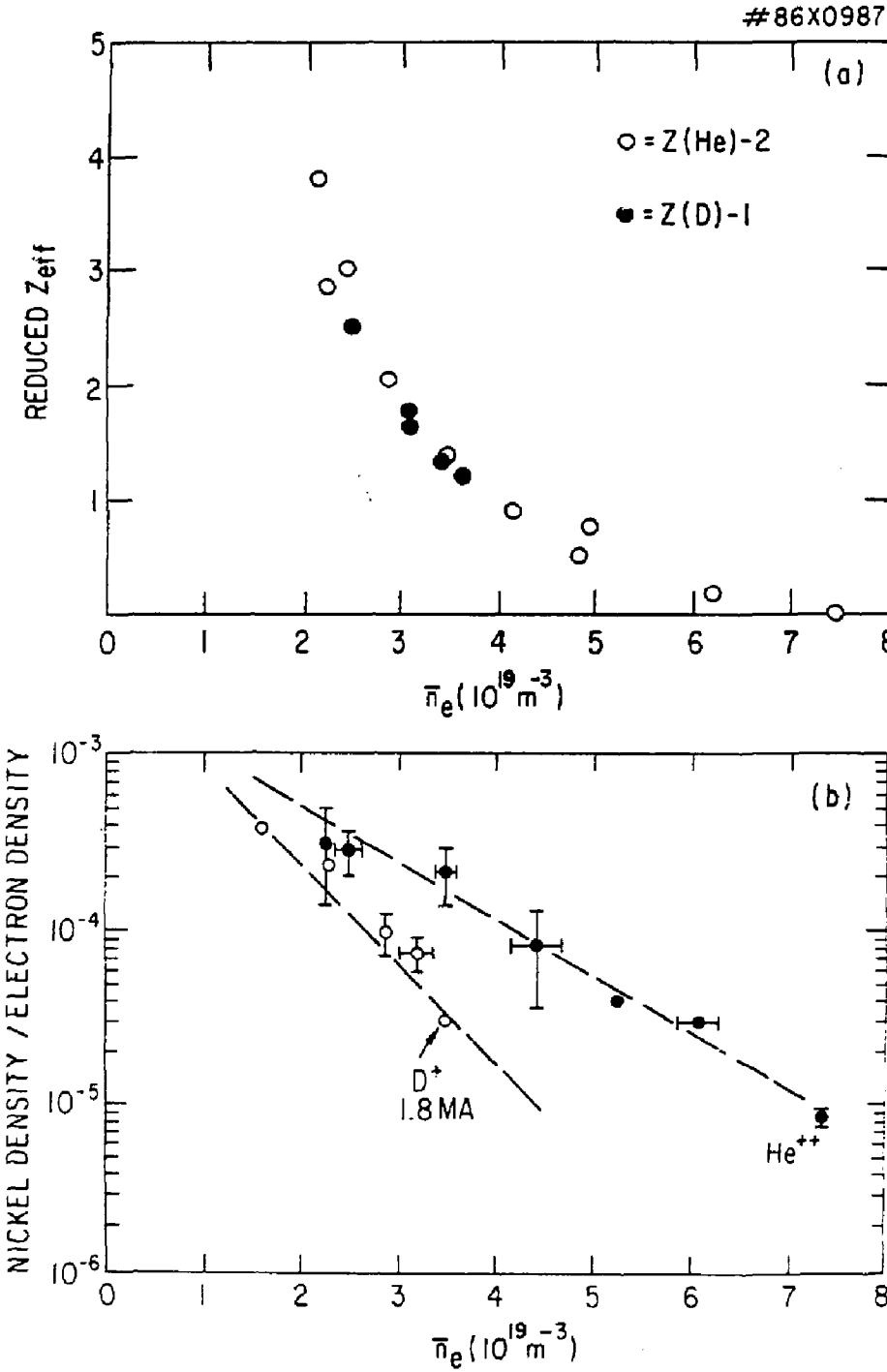
#86X0987
(a)
○ = Z(He)-2
● = Z(D)-1
REDUCED Z_{eff}
$\bar{n}_e(10^{19}m^{-3})$
(b)
NICKEL DENSITY / ELECTRON DENSITY
D^+
1.8 MA
He^{++}
$\bar{n}_e(10^{19}m^{-3})$

Fig. 7

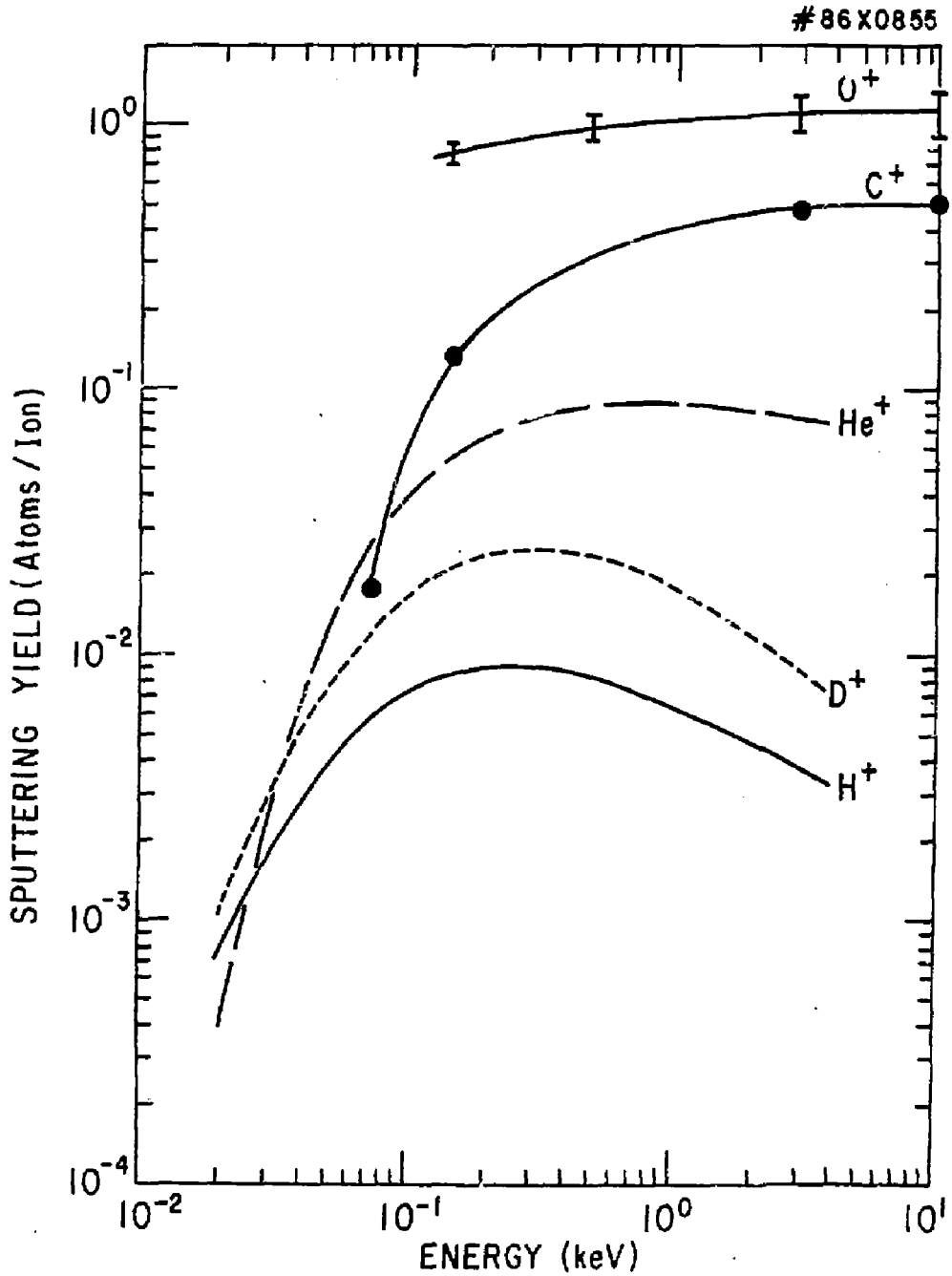
#86X0855
O+
C+
He+
D+
H+
SPUTTERING YIELD (Atoms / Ion)
ENERGY (keV)
10^0
10^-1
10^-2
10^-3
10^-4
10^-2
10^-1
10^0
10^1

Fig. 8

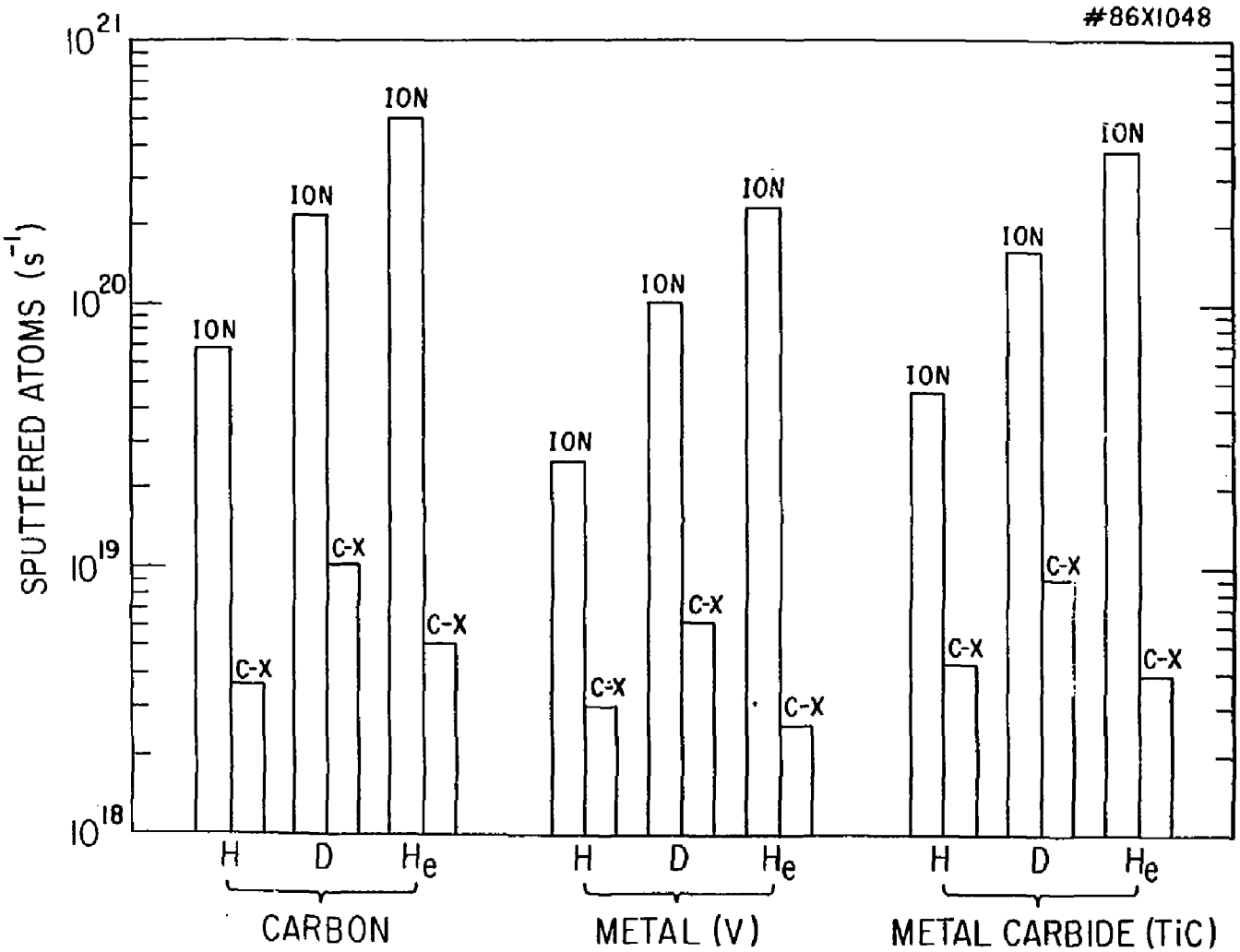
#86X1048
SPUTTERED ATOMS (s^{-1})
10^{21}
10^{20}
10^{19}
10^{18}
ION
C-X
H
D
He
CARBON
METAL (V)
METAL CARBIDE (TiC)

Fig. 9

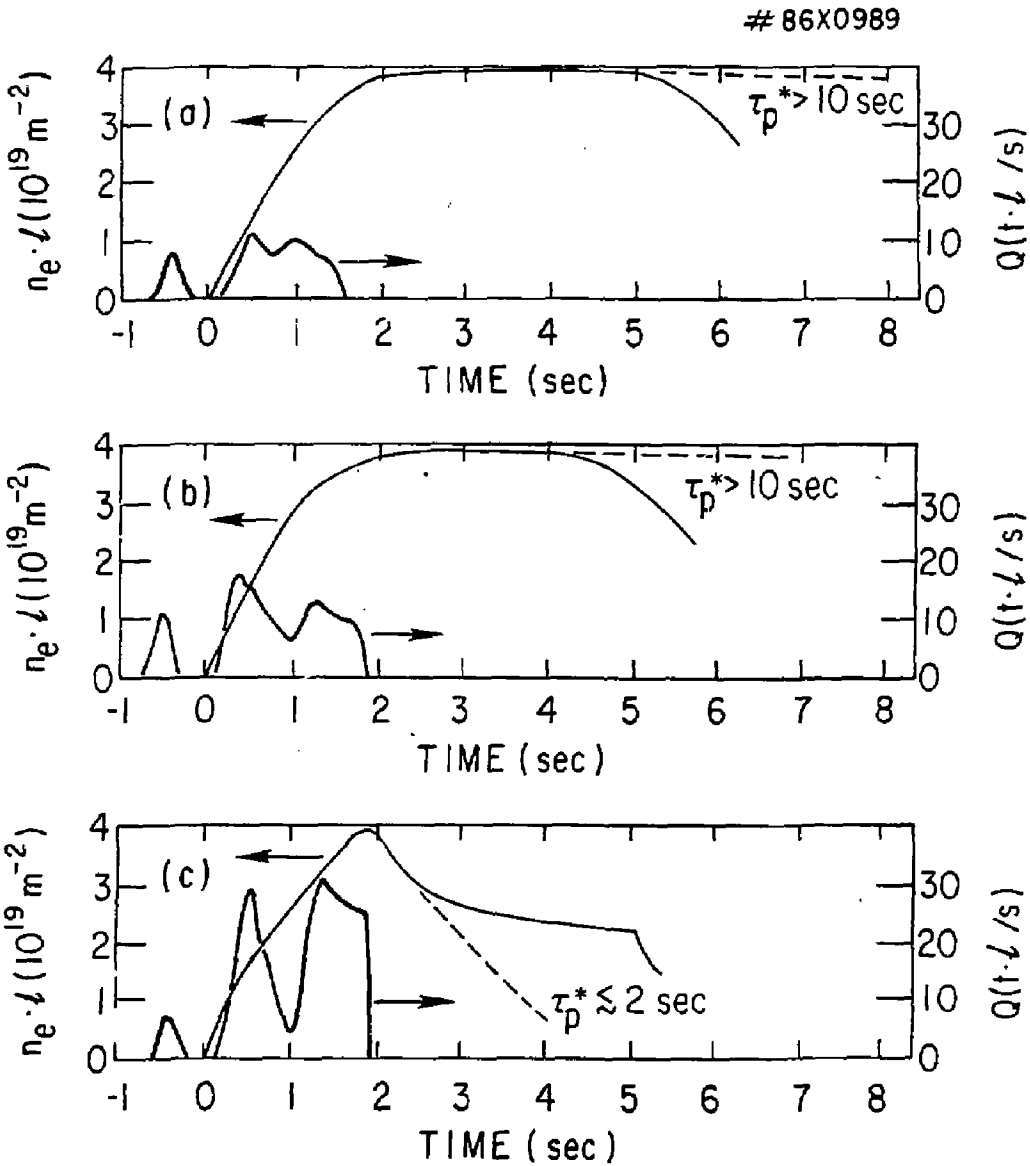
#86X0989
(a)
$\tau_p^* > 10$ sec
(b)
$\tau_p^* > 10$ sec
(c)
$\tau_p^* \lesssim 2$ sec
$n_e \cdot \ell\ (10^{19} m^{-2})$
$Q(t \cdot \ell / s)$
TIME (sec)

Fig. 10

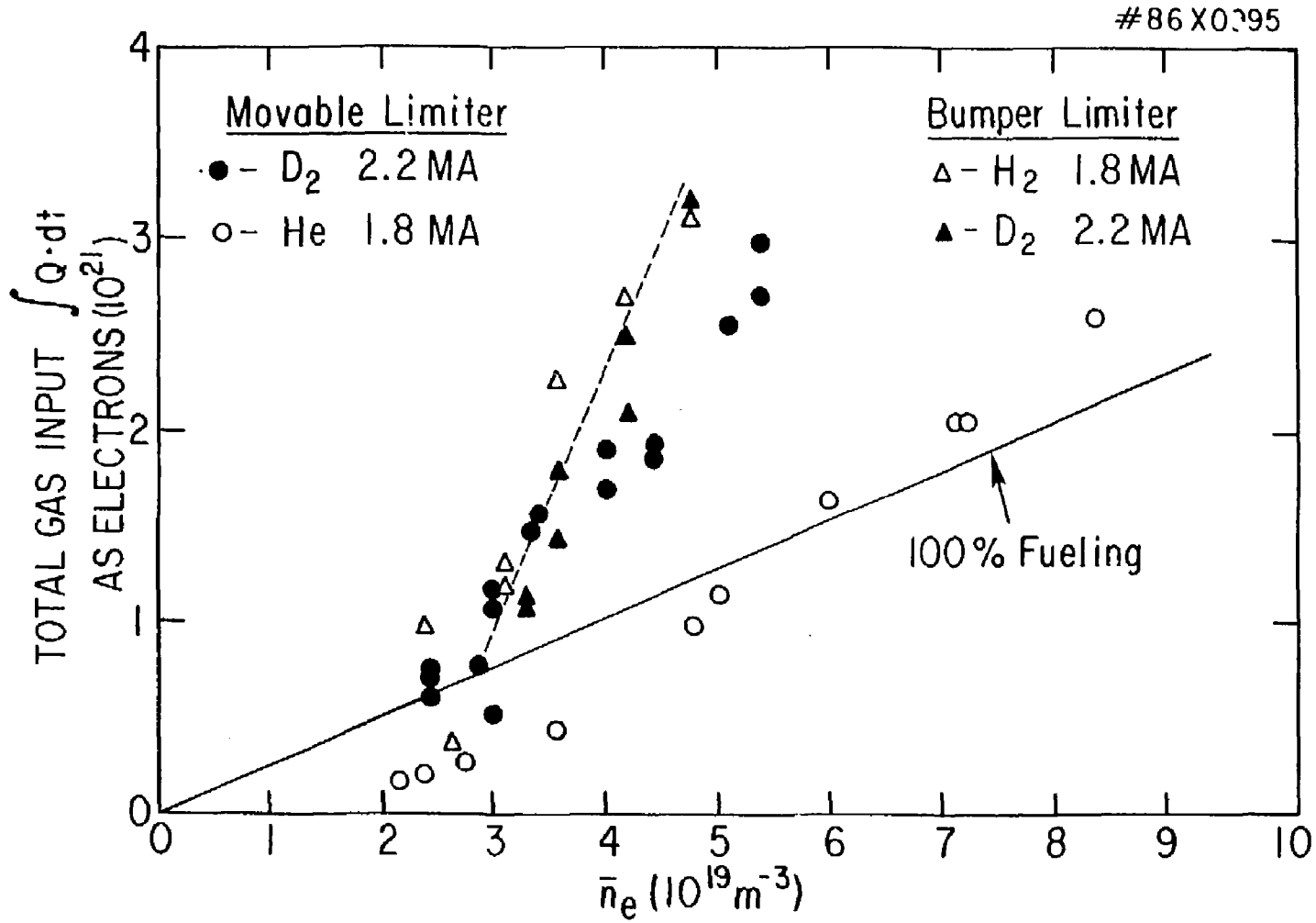
#86X0295
Movable Limiter
● - D2 2.2 MA
○ - He 1.8 MA
Bumper Limiter
△ - H2 1.8 MA
▲ - D2 2.2 MA
100% Fueling
TOTAL GAS INPUT ∫Q·dt AS ELECTRONS (10^21)
n̄e (10^19 m^-3)
0
1
2
3
4
5
6
7
8
9
10

Fig. 11

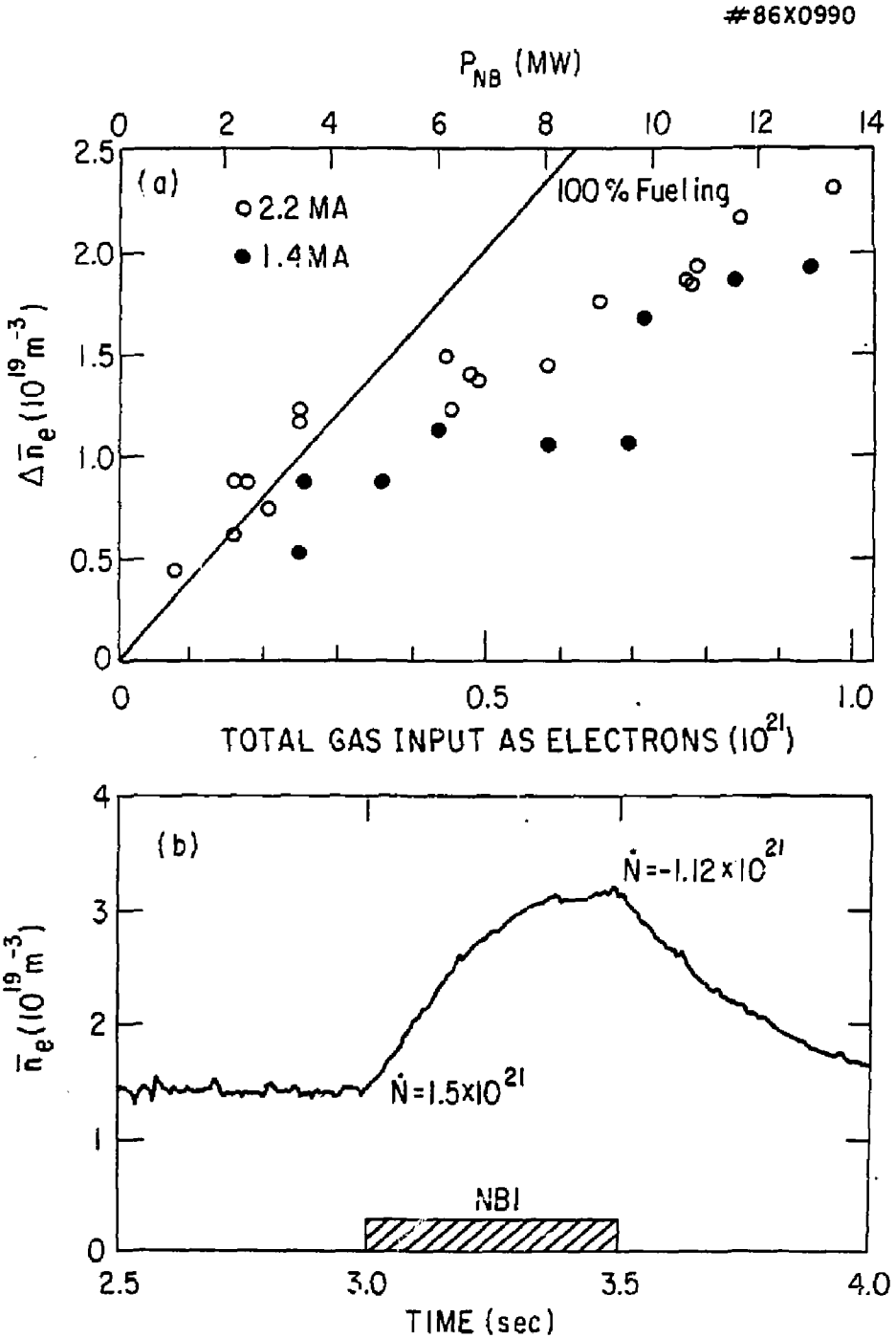
#86X0990
P_NB (MW)
0
2
4
6
8
10
12
14
2.5
2.0
1.5
1.0
0.5
0
(a)
o 2.2 MA
• 1.4 MA
100 % Fueling
Δ n̄e (10^19 m^-3)
0
0.5
1.0
TOTAL GAS INPUT AS ELECTRONS (10^21)
4
3
2
1
0
(b)
Ṅ=-1.12x10^21
Ṅ=1.5x10^21
NBI
n̄e (10^19 m^-3)
2.5
3.0
3.5
4.0
TIME (sec)

Fig. 12

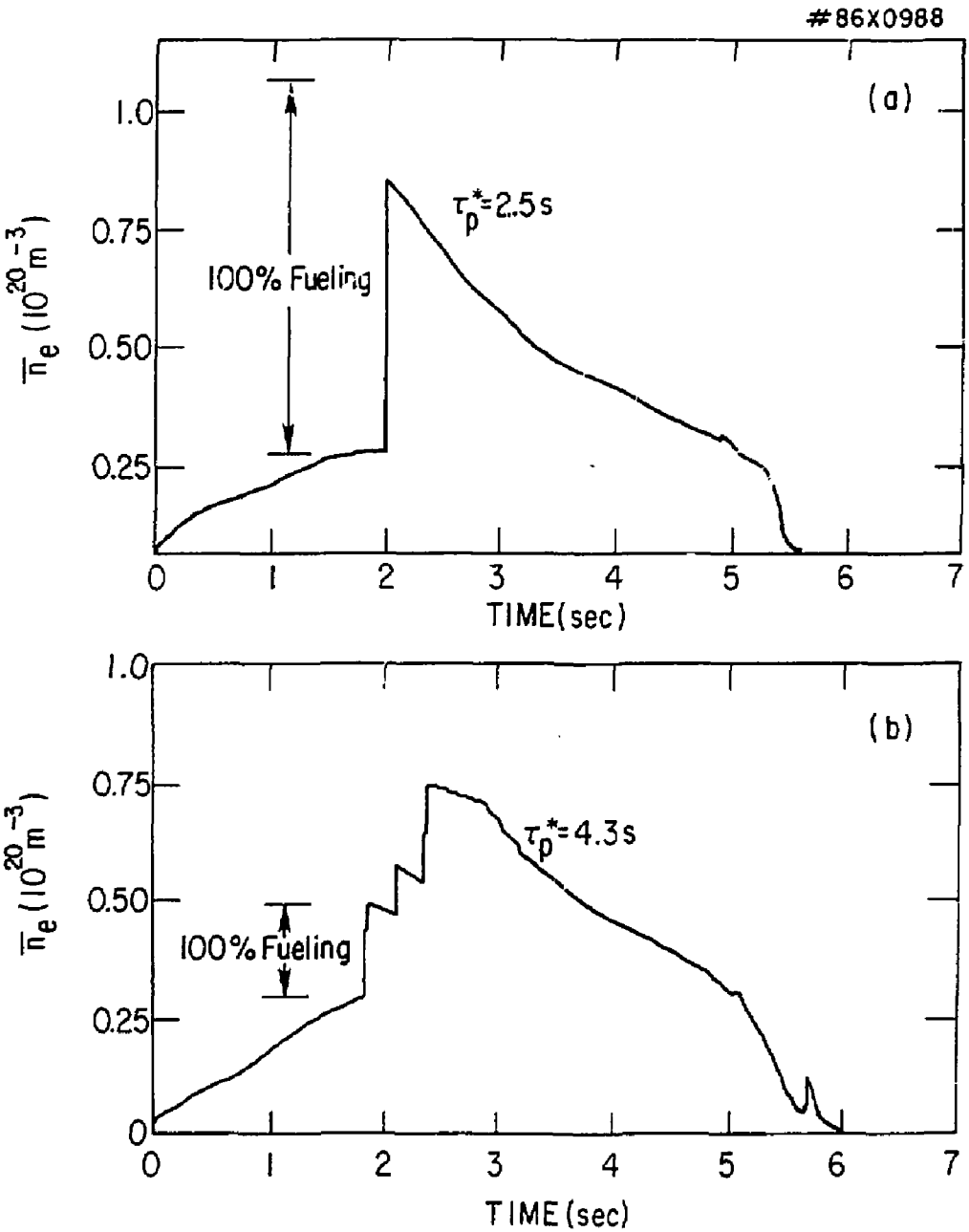
#86X0988
(a)
1.0
0.75
0.50
0.25
$\bar{n}_e$ (10^{20} m^{-3})
100% Fueling
τ_p^*=2.5s
0
1
2
3
4
5
6
7
TIME(sec)
(b)
1.0
0.75
0.50
0.25
0
$\bar{n}_e$ (10^{20} m^{-3})
100% Fueling
τ_p^*=4.3s
0
1
2
3
4
5
6
7
TIME (sec)

Fig. 13

EXTERNAL DISTRIBUTION IN ADDITION TO UC-20

Plasma Res Lab, Austra Nat'l Univ, AUSTRALIA
Dr. Frank J. Paoloni, Univ of Wollongong, AUSTRALIA
Prof. I.R. Jones, Flinders Univ., AUSTRALIA
Prof. M.H. Brennan, Univ Sydney, AUSTRALIA
Prof. F. Cap, Inst Theo Phys, AUSTRIA
M. Goossens, Astronomisch Instituut, BELGIUM
Prof. R. Boucique, Laboratorium voor Natuurkunde, BELGIUM
Dr. D. Palumbo, Dg XII Fusion Prog, BELGIUM
Ecole Royale Militaire, Lab de Phys Plasmas, BELGIUM
Dr. P.H. Sakanaka, Univ Estadual, BRAZIL
Lib. & Doc. Div., Instituto de Pesquises Espaciais, BRAZIL
Dr. C.R. James, Univ of Alberta, CANADA
Prof. J. Teichmann, Univ of Montreal, CANADA
Dr. H.M. Skarsgard, Univ of Saskatchewan, CANADA
Prof. S.R. Sreenivasan, University of Calgary, CANADA
Prof. Tudor W. Johnston, INRS-Energie, CANADA
Dr. Hannes Barnard, Univ British Columbia, CANADA
Dr. M.P. Bachynski, MPB Technologies, Inc., CANADA
Chalk River, Nucl Lab, CANADA
Zhengwu Li, SW Inst Physics, CHINA
Library, Tsing Hua University, CHINA
Librarian, Institute of Physics, CHINA
Inst Plasma Phys, Academia Sinica, CHINA
Dr. Peter Lukac, Komenskeho Univ, CZECHOSLOVAKIA
The Librarian, Culham Laboratory, ENGLAND
Prof. Schatzman, Observatoire de Nice, FRANCE
J. Radet, CEN-BP6, FRANCE
JET Reading Room, JET Joint Undertaking, ENGLAND
AM Dupas Library, AM Dupas Library, FRANCE
Dr. Tom Mual, Academy Bibliographic, HONG KONG
Preprint Library, Cent Res Inst Phys, HUNGARY
Dr. R.K. Chhajlani, Vikram Univ, INDIA
Dr. B. Dasgupta, Saha Inst, INDIA
Dr. P. Kaw, Physical Research Lab, INDIA
Dr. Phillip Rosenau, Israel Inst Tech, ISRAEL
Prof. S. Cuperman, Tel Aviv University, ISRAEL
Prof. G. Rostagni, Univ Di Padova, ITALY
Librarian, Int'l Ctr Theo Phys, ITALY
Miss Clelia De Palo, Assoc EURATOM-ENEA, ITALY
Biblioteca, del CNR EURATOM, ITALY
Dr. H. Yamato, Toshiba Res & Dev, JAPAN
Direc. Dept. Lg. Tokamak Dev, JAERI, JAPAN
Prof. Nobuyuki Inoue, University of Tokyo, JAPAN
Research Info Center, Nagoya University, JAPAN
Prof. Kyoji Nishikawa, Univ of Hiroshima, JAPAN
Prof. Sigeru Mori, JAERI, JAPAN
Prof. S. Tanaka, Kyoto University, JAPAN
Library, Kyoto University, JAPAN
Prof. Ichiro Kawakami, Nihon Univ, JAPAN
Prof. Satoshi Itoh, Kyushu University, JAPAN
Dr. D.I. Choi, Adv. Inst Sci & Tech, KOREA
Tech Info Division, KAERI, KOREA
Bibliotheek, Fom-Inst Voor Plasma, NETHERLANDS
Prof. B.S. Liley, University of Waikato, NEW ZEALAND
Prof. J.A.C. Cabral, Inst Superior Tecn, PORTUGAL
Dr. Octavian Petrus, ALI CUZA University, ROMANIA
Prof. M.A. Hellberg, University of Natal, SO AFRICA
Dr. Johan de Villiers, Plasma Physics, Nucor, SO AFRICA
Fusion Div. Library, JEN, SPAIN
Prof. Hans Wilhelmson, Chalmers Univ Tech, SWEDEN
Dr. Lennart Stenflo, University of UMEA, SWEDEN
Library, Royal Inst Tech, SWEDEN
Centre de Recherchesen, Ecole Polytech Fed, SWITZERLAND
Dr. V.T. Tolok, Kharkov Phys Tech Ins, USSR
Dr. D.D. Ryutov, Siberian Acad Sci, USSR
Dr. G.A. Eliseev, Kurchatov Institute, USSR
Dr. V.A. Glukhikh, Inst Electro-Physical, USSR
Institute Gen. Physics, USSR
Prof. T.J.M. Boyd, Univ College N Wales, WALES
Dr. K. Schindler, Ruhr Universitat, W. GERMANY
ASDEX Reading Rm, IPP/Max-Planck-Institut fur Plasmaphysik, F.R.G.
Nuclear Res Estab, Julich Ltd, W. GERMANY
Librarian, Max-Planck Institut, W. GERMANY
Bibliothek, Inst Plasmaforschung, W. GERMANY
Prof. R.K. Janev, Inst Phys, YUGOSLAVIA